Journal of Scientific Computing (2026) 106:46
https://doi.org/10.1007/s10915-025-03169-5

An Efficient Spectral Method for Fourth-Order PDEs in Complex Geometries

Jie Shen[1] · **Xian Wen**[2]

Received: 24 September 2025 / Revised: 10 December 2025 / Accepted: 14 December 2025

Abstract
Building upon the fictitious domain approach recently introduced by Gu and Shen [17, 18] for second-order equations, we construct an efficient spectral formulation for solving fourth-order boundary value problems in 2D complex geometries. By embedding irregular regions into a disk, we reduce the two-dimensional fourth-order problem to a series of one-dimensional, fourth-order equations with constant coefficients, which can be solved efficiently by a spectral method, plus a least squares problem, which is essentially one-dimensional, to enforce the boundary conditions. To overcome the ill-conditioning of the least squares problem, a robust Tikhonov-regularized least-squares formulation is used to ensure numerical stability. The method preserves the simplicity of the original differential operator and leads to fast and accurate solvers for fourth-order problems in complex domains. Extensive numerical results demonstrate the fast convergence and broad applicability of our method, showcased by successful solutions to the generalized Stokes problem and the Cahn-Hilliard equation.

Keywords Spectral method · Fictitious domain · Fourth-order equation · Stokes problem · Cahn-Hilliard equation

Mathematics Subject Classification 65N35 · 65N85 · 35J40 · 76D07

1 Introduction

We consider in this paper numerical solution of the following fourth-order partial differential equations (PDEs)

✉ Jie Shen
jshen@eitech.edu.cn

✉ Xian Wen
math31wx@163.com

[1] School of Mathematical Sciences, Eastern Institute of Technology, Ningbo, Zhejiang 315200, P. R. China

[2] School of Mathematical Sciences, Shanghai Jiao Tong University, Shanghai 200240, P. R. China

Published online: 17 January 2026

$$\begin{aligned} \alpha V - \beta \Delta V + \Delta^2 V &= F, && \text{in } \Omega, \\ V &= G, && \text{on } \partial\Omega, \\ \frac{\partial V}{\partial \mathbf{n}} &= H, && \text{on } \partial\Omega, \end{aligned} \tag{1.1}$$

where $\Omega \in \mathbb{R}^2$ and α, β are non-negative coefficients. The above problem arises in many applications in science and engineering, such as the biharmonic equation, the stream-function formulation of the Stokes equations, and time discretization of fourth-order nonlinear parabolic equations such as the Cahn-Hilliard and Kuramoto-Sivashinsky equations. Thus, it is important to develop efficient and accurate numerical methods for (1.1). While traditional low-order approaches such as finite difference [34] or finite element methods (FEM) [12] are flexible in handling complex geometries, they typically require very fine meshes to achieve high accuracy, leading to high computational costs. Furthermore, for fourth-order problems, standard conforming FEM formulations need to use C^1-continuous elements, which is difficult and adds significant implementation complexity.

Spectral methods are capable of achieving exponential convergence for smooth solutions in regular domains[6, 9, 19, 29, 32, 36], and have been successfully used to solve fourth-order problems [3, 5, 20, 25, 30, 37, 43]. However, it should be noted that even for regular domains, solving (1.1), which is non separable, with spectral method is much more difficult than solving second-order separable equations. Moreover, classical spectral methods are restricted to regular domains, and extending them to complex geometries presents significant challenges. Currently, there are primarily two commonly used approaches for extending spectral methods to problems in complex domains. The first approach is to map a complex domain into a regular domain through a mapping [27], e.g., the Gordon-Hall mapping [15]. The second approach involves embedding a complex domain into a larger regular region, classified as fictitious domain methods [7]. We should also note that Trefethen and his collaborators [13, 14] recently developed the so called lightning algorithm which uses rational approximation to efficiently approximate solutions of Laplace and homogeneous Helmholtz equations in two-dimensional polygonal domains.

The mapping approach was pioneered by Orszag [27], who employed a Fourier-Chebyshev method with explicit mappings for annular regions; recently, Wang et al. [38] introduced a spectral-Galerkin method with a rigorous error analysis for 2D curved domains using polar coordinate transformations; this framework was subsequently adapted for exterior problems with complex obstacles [41]; building on these advances, Yao et al. [40] tackled two-body problems by designing a conforming multi-domain spectral method and an extension to 3D is attempted in Yao et al. [42] with a new spherical coordinate-based transformation.

However, the mapping approach faces severe difficulties when applied to fourth-order PDEs, as the transformation of the bi-Laplacian operator (Δ^2) leads to a complex variable-coefficient equation. While a rigorous theoretical analysis for this transformed equation can be established under more strict smoothness conditions on the boundary (following ideas in [38]), the practical challenges are significant. The transformation not only complicates the implementation but, more importantly, results in dense and ill-conditioned matrices that severely affect computational efficiency and stability.

The fictitious domain (or embedding) approach embeds a complex domain Ω into a larger, regular domain, thereby avoiding body-fitted meshing and complex coordinate transformations. This approach has been frequently used in finite-element [11] or finite difference [4] contexts, but it suffers from low convergence rates. Recently, Gu and Shen developed a circular embedding spectral method for second-order elliptic PDEs [17] and Helmholtz equation [18], and showed that it can achieve spectral accuracy, and easy to implement than the rect-

angular embedding approach in [16]. However, to enforce the boundary condition, it requires to solve a least squares problem which can be very ill conditioned and limits the accuracy that can be obtained and the size of the problem that can be solved.

The main goal of this paper is to extend the circular embedding strategy to solve fourth-order PDEs in complex geometries, and in the meantime, to propose an efficient approach to alleviate the ill conditioning associated with the least squares problem. In particular, we develop a framework that achieves a near-perfect decoupling of the fourth-order PDEs from the intricate boundary conditions. Specifically, the solution process is split into two stages. In the first stage, we solve a set of one-dimensional, constant-coefficient fourth-order ODEs in the radial direction of the extended domain. These equations serve as a basis for the final solution and are solved efficiently using standard spectral methods, entirely independent to the shape or location of the physical boundary $\partial\Omega$. In the second stage, the solution to the original problem (1.1) is constructed as an explicit linear combination of these basis solutions. The unknown coefficients of this expansion can then be determined by enforcing the original boundary conditions in a least-squares sense. This elegant procedure confines the intricate geometric information to a small, well-conditioned linear system, while the bulk of the computational effort is spent on solving simple one dimensional PDEs.

The proposed circular embedding method for solving fourth-order problems in complex geometries is highly effective and robust. Its advantages are threefold.

- Firstly, the method preserves the constant coefficients of the original PDE operator, enabling the decomposition of a two-dimensional problem into a sequence of one-dimensional problems that can be solved with exceptional efficiency by established spectral algorithms, plus a small linear system to enforce the boundary conditions. Thus its computational and implementional complexity is essentially the same as the standard spectral methods for solving fourth-order problems in a rectangular domain [30].
- Secondly, the approach can be applied to any simply connected domain, offering significant geometric flexibility.
- Thirdly, the boundary conditions are enforced via a Tikhonov-regularized least-squares formulation which proves to be highly robust, permitting the use of a large number of collocation points on the boundary to ensure high accuracy without sacrificing the numerical stability.

The remainder of this paper is organized as follows. In Section 2, we detail the construction of the extended problem and the numerical discretization. Section 3 presents numerical examples that validate the accuracy and robustness of our method, including an application to the generalized Stokes problem. In Section 4, we present the extension to the fourth-order problems with Neumann boundary conditions, and as an application, apply it to solve the Cahn-Hilliard equation. The final section contains some concluding remarks.

We now present some of the notations to be used in the sequel. We define the scaled Jacobi weight function,

$$\hat{\omega}^{\alpha,\beta}(r) = (1-r)^{\alpha} r^{\beta}, \quad 0 < r < 1, \tag{1.2}$$

and the weighted L^2 inner product,

$$(u, v)_{\hat{\omega}^{\alpha,\beta}} = \int_0^1 u(r)\overline{v}(r)\hat{\omega}^{\alpha,\beta}(r)\mathrm{d}r. \tag{1.3}$$

The corresponding weighted L^2, H^1 and H^2 spaces are defined by

$$H^m_{\hat{\omega}^{\alpha,\beta}} = \left\{u(r) : \partial_r^k u \in L^2_{\hat{\omega}^{\alpha,\beta}}, 0 \le k \le m\right\}, \tag{1.4}$$

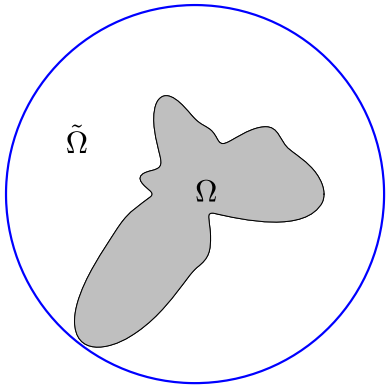

Fig. 1 The original domain Ω and the enclosing circle $\tilde{\Omega}$

equipped with norms

$$\|u\|_{m,\hat{\omega}^{\alpha,\beta}} = \left(\sum_{k=0}^{m} \|\partial_r^k u\|^2_{\hat{\omega}^{\alpha,\beta}}\right)^{\frac{1}{2}}. \tag{1.5}$$

In particular, we set $(\cdot,\cdot) = (\cdot,\cdot)_{\hat{\omega}^{0,0}}$, $\|\cdot\| = \|\cdot\|_{\hat{\omega}^{0,0}}$.

2 Problem Formulation and its Approximation

In this section, we first describe the formulation of the problem using circular embedding and its subsequent decomposition through polar transformation, followed by the Petrov-Galerkin formulation for both the spatial continuous and discrete cases.

2.1 Problem Formulation and a Conceptual Algorithm

Similar to the strategy outlined in [17], we embed the complex geometry into a disk and subsequently apply the classical spectral method to the extended domain.

Consider the fourth-order problem (1.1). Let $\tilde{\Omega}$ be a circular domain that encloses Ω, such that $\Omega \subset\subset \tilde{\Omega}$ (see Figure 1). In this work, we assume that the source term F has been successfully extended to the larger domain $\tilde{\Omega}$. The existence and construction of such smooth extensions are well-documented in the literature [1, 2, 22, 26]. Furthermore, Huybrechs [22] provides a rigorous treatment of extensions in complex geometries, such as non-star-shaped and non-simply connected domains. Let U be the solution to the following extended problem defined in $\tilde{\Omega}$:

$$\begin{aligned} \alpha U - \beta\Delta U + \Delta^2 U &= F, && \text{in } \tilde{\Omega},\\ U &= G, && \text{on } \partial\Omega,\\ \frac{\partial U}{\partial \mathbf{n}} &= H, && \text{on } \partial\Omega. \end{aligned} \tag{2.1}$$

It follows that for any solution of (2.1), we have $U|_{\Omega} = V$. In other word, its restriction on Ω is the solution of the original problem (1.1). Thus, our goal is to find a solution of the extended problem (2.1) which is as smooth as the data allows.

Without loss of generality, we assume that $\tilde{\Omega} = \{(x, y) : x^2 + y^2 < 1\}$, which represents the interior of the unit circle. Let $\tilde{\Pi} = [0, 1] \times [0, 2\pi]$, and applying the polar transform

$\mathbb{T} : \bar{\Pi} \to \overline{\overline{\Omega}}$ to the problem (2.1):

$$\begin{aligned} u(r,\theta) &:= U(r\cos(\theta), r\sin(\theta)), \quad f(r,\theta) := F(r\cos(\theta), r\sin(\theta)), \\ g(r,\theta) &:= G(r\cos(\theta), r\sin(\theta)), \quad h(r,\theta) := H(r\cos(\theta), r\sin(\theta)). \end{aligned} \tag{2.2}$$

Then, the problem (2.1) is transformed into:

$$\begin{aligned} \alpha u - \beta \mathcal{L} u + \mathcal{L}^2 u &= f, && (r,\theta) \in \Pi, \\ u_\theta(0,\theta) &= 0, && u \text{ is periodic in } \theta, \\ u &= g, && \text{on } \Gamma, \\ \partial_r u &= h, && \text{on } \Gamma, \end{aligned} \tag{2.3}$$

where $\Gamma = \mathbb{T}^{-1}(\partial\Omega)$, and the differential operator is given by

$$\mathcal{L} u = \frac{1}{r}\frac{\partial}{\partial r}\left(r\frac{\partial u}{\partial r}\right) + \frac{1}{r^2}\frac{\partial^2 u}{\partial \theta^2}. \tag{2.4}$$

Next, we expand u and f in Fourier series in θ direction,

$$u(r,\theta) = \sum_{|m|=0}^{\infty} u_m(r) e^{\mathrm{i}m\theta}, \quad f(r,\theta) = \sum_{|m|=0}^{\infty} f_m(r) e^{\mathrm{i}m\theta}. \tag{2.5}$$

Substituting the Fourier series expansion (2.5) into (2.3), we find that the two-dimensional problem can be reduced to a sequence of one dimensional ODEs for the expansion coefficients $u_m(r)$:

$$\alpha u_m(r) - \beta \mathcal{L}_m u_m(r) + \mathcal{L}_m^2 u_m(r) = f_m(r), \quad 0 < r < 1, \tag{2.6}$$

with one-sided pole conditions [24]:

$$\begin{aligned} \partial_r u_m(0) &= 0, && \text{if } m = 0, \\ u_m(0) &= 0, && \text{if } |m| = 1, \\ u_m(0) = \partial_r u_m(0) &= 0, && \text{if } |m| \geq 2, \end{aligned} \tag{2.7}$$

and the operator $\mathcal{L}_m$ is defined as

$$\mathcal{L}_m u = \frac{1}{r}\frac{\partial}{\partial r}\left(r\frac{\partial u}{\partial r}\right) - \frac{m^2}{r^2} u. \tag{2.8}$$

By direct calculations,

$$\mathcal{L}_m^2 u = \partial_r^4 u + \frac{2}{r}\partial_r^3 u - \frac{1+2m^2}{r^2}\partial_r^2 u + \frac{1+2m^2}{r^3}\partial_r u + \frac{m^4 - 4m^2}{r^4} u. \tag{2.9}$$

Note that the system (2.6)–(2.7) is undetermined since there are no boundary conditions specified at $r = 1$. To arrive at a well-posed system for $u_m(r)$, we set:

$$u_m(1) = t_m, \quad \partial_r u_m(1) = s_m, \quad |m| = 0, 1, \ldots \tag{2.10}$$

where constants $\{t_m\}$ and $\{s_m\}$ are undetermined parameters to be used to enforce the boundary conditions:

$$u = g, \quad \partial_r u = h \quad \text{on } \Gamma. \tag{2.11}$$

To achieve this, we can appropriately decompose the original problem into three mutually independent subproblems. This decomposition ensures that the solution to the original problem can be expressed as the sum of the solutions to these three subproblems. More

specifically, given the constants $\{t_m\}$ and $\{s_m\}$, the solution $u_m(r)$ can be explicitly derived as follows:

$$u_m(r; t_m, s_m) = t_m\phi_m(r) + s_m\varphi_m(r) + \psi_m(r), \tag{2.12}$$

where $\phi_m(r)$ is the solution of

$$\begin{aligned} &\alpha\phi_m(r) - \beta\mathcal{L}_m\phi_m(r) + \mathcal{L}_m^2\phi_m(r) = 0, \quad 0 < r < 1, \\ &\text{with pole conditions as specified in (2.7)}; \quad \phi_m(1) = 1, \quad \partial_r\phi_m(1) = 0, \end{aligned} \tag{2.13}$$

$\varphi_m(r)$ is the solution of

$$\begin{aligned} &\alpha\varphi_m(r) - \beta\mathcal{L}_m\varphi_m(r) + \mathcal{L}_m^2\varphi_m(r) = 0, \quad 0 < r < 1, \\ &\text{with pole conditions as specified in (2.7)}; \quad \varphi_m(1) = 0, \quad \partial_r\varphi_m(1) = 1, \end{aligned} \tag{2.14}$$

and $\psi_m(r)$ is the solution of

$$\begin{aligned} &\alpha\psi_m(r) - \beta\mathcal{L}_m\psi_m(r) + \mathcal{L}_m^2\psi_m(r) = f_m(r), \quad 0 < r < 1, \\ &\text{with pole conditions as specified in (2.7)}; \quad \psi_m(1) = 0, \quad \partial_r\psi_m(1) = 0. \end{aligned} \tag{2.15}$$

Remark 2.1 For problems (2.13)–(2.14), a homogenization technique can be employed, allowing the original solution to be obtained by solving a homogeneous problem. For example, the function $\tilde{\phi}_m(r) = \phi_m(r) - r^2(3-2r)$ satisfies the following equation with homogeneous boundary conditions after homogenization:

$$\begin{aligned} &\alpha\tilde{\phi}_m(r) - \beta\mathcal{L}_m\tilde{\phi}_m(r) + \mathcal{L}_m^2\tilde{\phi}_m(r) = -\tilde{f}_m(r), \quad 0 < r < 1, \\ &\text{with pole conditions as specified in (2.7)}; \quad \tilde{\phi}_m(1) = \partial_r\tilde{\phi}_m(1) = 0, \end{aligned} \tag{2.16}$$

where

$$\tilde{f}_m(r) = \alpha r^2(3-2r) + \beta\left(-2r(m^2-9) + 3(m^2-4)\right) - \frac{2(m^2-1)(m^2-9)}{r} + \frac{3m^2(m^2-4)}{r^2}. \tag{2.17}$$

The function $\tilde{f}_m(r)$ may appear to exhibit a singularity at $r = 0$, but when we take the inner product $(\tilde{f}_m(r), v)_{\tilde{\omega}^{0,1}}$, this singularity will vanish since the test function v satisfies the pole conditions specified in (2.7).

Remark 2.2 As the solutions $\phi_m(r)$ and $\varphi_m(r)$ are independent of Ω and the function F, we can treat solving (2.13)–(2.14) as a pre-computation, which can be efficiently solved using a spectral-Galerkin approach, as described in [24, 30, 31].

It remains to determine $\{t_m\}$ and $\{s_m\}$. The key issue is to choose appropriate $\{t_m\}$ and $\{s_m\}$ such that u satisfies the boundary conditions (2.11). Specifically, suppose Γ is parameterized by

$$\Gamma = \{(\rho(\theta), \theta) : 0 \le \theta < 2\pi\}, \tag{2.18}$$

then we can show that the boundary condition (2.11) is equivalent to:

$$\begin{aligned} &\big(u(\rho(\theta),\theta) - g(\rho(\theta),\theta),\xi(\theta)\big)_{[0,2\pi)} = 0, \quad \forall\, \xi(\theta) \in L^2[0,2\pi), \\ &\big(\partial_r u(\rho(\theta),\theta) - h(\rho(\theta),\theta),\xi(\theta)\big)_{[0,2\pi)} = 0, \quad \forall\, \xi(\theta) \in L^2[0,2\pi). \end{aligned} \tag{2.19}$$

Substituting (2.5) and (2.12) into these conditions and choosing the test functions $\xi(\theta) = e^{\mathrm{i}k\theta}$ yields, for each integer k:

$$\begin{aligned}
&\sum_{|m|=0}^{\infty} \int_0^{2\pi} \big(t_m \phi_m(\rho(\theta)) + s_m \varphi_m(\rho(\theta)) + \psi_m(\rho(\theta))\big) e^{\mathrm{i}(m-k)\theta} \mathrm{d}\theta = \int_0^{2\pi} g(\rho(\theta),\theta) e^{-\mathrm{i}k\theta} \mathrm{d}\theta, \\
&\sum_{|m|=0}^{\infty} \int_0^{2\pi} \partial_r \big(t_m \phi_m(\rho(\theta)) + s_m \varphi_m(\rho(\theta)) + \psi_m(\rho(\theta))\big) e^{\mathrm{i}(m-k)\theta} \mathrm{d}\theta = \int_0^{2\pi} h(\rho(\theta),\theta) e^{-\mathrm{i}k\theta} \mathrm{d}\theta.
\end{aligned} \tag{2.20}$$

Remark 2.3 The system (2.20) does not impose any smoothness requirement on the boundary function $\rho(\theta)$. In contrast, the mapping method for the fourth-order problem will require a higher regularity condition on $\rho(\theta)$.

2.2 Continuous Petrov–Galerkin Formulation

We now derive the continuous Petrov-Galerkin formulation corresponding to the method outlined in subsection 2.1, tailored for the extended two-dimensional problem (2.3). To this end, we introduce the following one-dimensional Hilbert spaces:

$$\begin{aligned}
\hat{W}^0 &= \Big\{ u(r) \Big|\, u'(0) = 0, \int_0^1 r|\partial_r^2 u|^2 + \frac{1}{r}|\partial_r u|^2 + r|u|^2 \mathrm{d}r < \infty \Big\}, \\
\hat{W}^m &= \Big\{ u(r) \Big|\, u(0) = 0, \int_0^1 r|\partial_r^2 u|^2 + \frac{1}{r^2}|\partial_r u - \frac{u}{r}|^2 + \frac{3}{r^2}|u|^2 \mathrm{d}r < \infty \Big\}, \ |m| = 1, \\
\hat{W}^m &= \Big\{ u(r) \Big|\, u(0) = u'(0) = 0, \int_0^1 r|\partial_r^2 u|^2 + \frac{2m^2+1}{r}|\partial_r u|^2 + \frac{m^4 - 4m^2}{r^3}|u|^2 \mathrm{d}r < \infty \Big\}, \ |m| > 1, \\
\hat{Y}^m &= \{ u \in \hat{W}^m \,|\, u(1) = u'(1) = 0 \}, \ \forall\, m,
\end{aligned} \tag{2.21}$$

equipped with the following norms:

$$\|u\|_{\hat{W}^m} := \begin{cases}
\big(\|\partial_r^2 u\|_{\hat{\omega}^{0,1}}^2 + \|\partial_r u\|_{\hat{\omega}^{0,-1}}^2 + \|u\|_{\hat{\omega}^{0,1}}^2 \big)^{\frac{1}{2}}, & m = 0, \\
\big(\|\partial_r^2 u\|_{\hat{\omega}^{0,1}}^2 + \|\partial_r u - \frac{u}{r}\|_{\hat{\omega}^{0,-2}}^2 + 3\|u\|_{\hat{\omega}^{0,-2}}^2 \big)^{\frac{1}{2}}, & |m| = 1, \\
\big(\|\partial_r^2 u\|_{\hat{\omega}^{0,1}}^2 + (2m^2+1)\|\partial_r u\|_{\hat{\omega}^{0,-1}}^2 + (m^4 - 4m^2)\|u\|_{\hat{\omega}^{0,-3}}^2 \big)^{\frac{1}{2}}, & |m| > 1.
\end{cases} \tag{2.22}$$

Then we define

$$W := \Big\{ u(r,\theta) = \sum_{|m|=0}^{\infty} u_m(r) e^{\mathrm{i}m\theta} \Big|\, u_m(r) \in \hat{W}^m, \sum_{|m|=0}^{\infty} \|u_m\|_{\hat{W}^m}^2 < \infty \Big\} \tag{2.23}$$

with norm

$$\|u\|_W := \Big(\sum_{|m|=0}^{\infty} \|u_m\|_{\hat{W}^m}^2 \Big)^{\frac{1}{2}}. \tag{2.24}$$

Next, we define the trial space X and test space Y as follows:

$$\begin{aligned}
X &:= \big\{ u \in W \,\big|\, u|_\Gamma = h, \quad \partial_r u|_\Gamma = g \big\}, \\
Y &:= \Big\{ v \in W \,\Big|\, v(r,\theta) = \sum_{|m|=0}^{\infty} v_m(r) e^{\mathrm{i}m\theta} \text{ with } v_m \in \hat{Y}^m \Big\}.
\end{aligned} \tag{2.25}$$

Note that we do not impose any boundary condition at $r = 1$ for the functions in the trial space X. This is essential for achieving spectral accuracy.

To formulate the variational problem, we define a bilinear form $\mathcal{A}(\cdot,\cdot) : X \times Y \to \mathbb{C}$ by

$$\mathcal{A}(u,v) := \sum_{|m|=0}^{\infty} A_m(u_m, v_m) := \sum_{|m|=0}^{\infty} \alpha\,(u_m, v_m)_{\hat{\omega}^{0,1}} + \beta\,(\partial_r u_m, \partial_r v_m)_{\hat{\omega}^{0,1}} + m^2\beta\,(u_m, v_m)_{\hat{\omega}^{0,-1}} + \left(\partial_r^2 u_m, \partial_r^2 v_m\right)_{\hat{\omega}^{0,1}} + (2m^2+1) b_m(u_m, v_m) + (m^4 - 4m^2)\,(u_m, v_m)_{\hat{\omega}^{0,-3}}\,, \tag{2.26}$$

where

$$b_m(u_m, v_m) = \begin{cases} (\partial_r u_m, \partial_r v_m)_{\hat{\omega}^{0,-1}}\,, & |m| \neq 1, \\ -\left(\partial_r^2 u_m, v_m\right)_{\hat{\omega}^{0,-1}} + (\partial_r u_m, v_m)_{\hat{\omega}^{0,-2}}\,, & |m| = 1. \end{cases} \tag{2.27}$$

We then consider the following weak formulation:

$$\begin{cases} \text{Find } u \in X \text{ such that} \\ \mathcal{A}(u,v) = (rf, v) \quad \forall v \in Y. \end{cases} \tag{2.28}$$

We demonstrate below that any solution obtained from the algorithm developed in the preceding subsection is indeed a solution to the weak problem presented above.

Proposition 2.4 *Let* $\{\phi_m\}$, $\{\varphi_m\}$, *and* $\{\psi_m\}$ *be the solutions of* (2.13)–(2.15), *and let*

$$u_m(r) = t_m \phi_m(r) + s_m \varphi_m(r) + \psi_m(r)$$

with $\{t_m\}$ *and* $\{s_m\}$ *satisfying* (2.20). *Then*

$$u(r,\theta) = \sum_{|m|=0}^{\infty} u_m(r) e^{\mathrm{i}m\theta}$$

is a solution of (2.28).

Proof By construction, each $u_m(r)$ satisfies the ODE (2.6) and the conditions $u_m(1) = t_m$ and $\partial_r u_m(1) = s_m$. It is also clear that $u_m \in \hat{W}^m$, which implies $u(r,\theta) = \sum_{|m|=0}^{\infty} u_m(r) e^{\mathrm{i}m\theta} \in W$.

For any test function $v = \sum_{|m|=0}^{\infty} v_m(r) e^{\mathrm{i}m\theta} \in Y$, we multiply equation (2.6) by $r v_m$ and integrate from $r = 0$ to $r = 1$. After performing integration by parts for each mode m, we obtain

$$A_m(u_m, v_m) = (f_m, v_m)_{\hat{\omega}^{0,1}}\,. \tag{2.29}$$

The boundary terms from the integration by parts vanish because the test function $v_m \in \hat{Y}^m$ satisfies $v_m(1) = \partial_r v_m(1) = 0$, and both the trial and test functions satisfy the necessary pole conditions at $r = 0$.

Summing (2.29) over all m directly yields $\mathcal{A}(u,v) = (rf, v)$.

It remains to show that $u \in X$. The construction of the system (2.20) ensures that the boundary conditions on Γ are satisfied:

$$u(\rho(\theta),\theta) = g(\rho(\theta),\theta) \quad \text{and} \quad \partial_r u(\rho(\theta),\theta) = h(\rho(\theta),\theta), \tag{2.30}$$

which implies $u \in X$. Thus, u is a solution of (2.28). □

2.3 Discrete Petrov-Galerkin Formulation

We construct below a discrete Petrov-Galerkin formulation corresponding to the weak problem (2.28). This formulation is essential for the numerical solution of the problem, as it discretizes the continuous weak form into a solvable system of equations.

First, we establish the spectral approximations to $\phi_m(r)$, $\varphi_m(r)$, and $\psi_m(r)$. Let $\hat{P}_N$ denote the set of all polynomials on $[0, 1]$ of degree no greater than N. Define the following spaces:

$$\begin{aligned} {}^1\hat{Y}_N^m &:= \{u \in \hat{W}^m \mid u(1) = 1, \quad \partial_r u(1) = 0\} \cap \hat{P}_N, \\ {}^2\hat{Y}_N^m &:= \{u \in \hat{W}^m \mid u(1) = 0, \quad \partial_r u(1) = 1\} \cap \hat{P}_N, \\ \hat{Y}_N^m &:= \hat{Y}^m \cap \hat{P}_N. \end{aligned} \tag{2.31}$$

We set $\hat{W}_N^m := \hat{W}^m \cap \hat{P}_N$, and let $\{\phi_{m,N}\} \in {}^1\hat{Y}_N^m$ be the solution of

$$\begin{aligned} &A_m(\phi_{m,N}, v_m) = 0, \quad \forall v_m \in \hat{Y}_N^m, \\ &\text{pole conditions: (2.7)}; \quad \phi_{m,N}(1) = 1, \quad \partial_r \phi_{m,N}(1) = 0, \end{aligned} \tag{2.32}$$

and let $\{\varphi_{m,N}\} \in {}^2\hat{Y}_N^m$ be the solution of

$$\begin{aligned} &A_m(\varphi_{m,N}, v_m) = 0, \quad \forall v_m \in \hat{Y}_N^m, \\ &\text{pole conditions: (2.7)}; \quad \varphi_{m,N}(1) = 0, \quad \partial_r \varphi_{m,N}(1) = 1, \end{aligned} \tag{2.33}$$

and let $\{\psi_{m,N}\} \in \hat{Y}_N^m$ be the solution of

$$\begin{aligned} &A_m(\psi_{m,N}, v_m) = (rf_m, v_m) \quad \forall v_m \in \hat{Y}_N^m, \\ &\text{pole conditions: (2.7)}; \quad \psi_{m,N}(1) = 0, \quad \partial_r \psi_{m,N}(1) = 0. \end{aligned} \tag{2.34}$$

Then, by the superposition principle, we can verify that $u_{m,N} = t_{m,N}\phi_{m,N}(r) + s_{m,N}\varphi_{m,N}(r) + \psi_{m,N}(r)$ is the solution of

$$A_m(u_{m,N}, v_m) = (rf_m, v_m) \quad \forall v_m \in \hat{Y}_N^m, \tag{2.35}$$

satisfying $u_{m,N}(1) = t_{m,N}$ and $\partial_r u_{m,N}(1) = s_{m,N}$ in $\hat{W}_N^m$.

We also define the discrete trial space by

$$\begin{aligned} X_{MN} := \Big\{ u_{MN}(r,\theta) = \sum_{|m|=0}^{M} u_{m,N}(r) e^{\mathrm{i}m\theta} \,\Big|\, u_{m,N} \in \hat{W}_N^m, \quad \left(u_{MN}, e^{\mathrm{i}k\theta}\right)_\Gamma = \left(g, e^{\mathrm{i}k\theta}\right)_\Gamma, \\ \left(\partial_r u_{MN}, e^{\mathrm{i}k\theta}\right)_\Gamma = \left(h, e^{\mathrm{i}k\theta}\right)_\Gamma, \quad |k| = 0, \cdots, M \Big\}. \end{aligned} \tag{2.36}$$

Let $u_{MN}(r,\theta) = \sum_{|m|=0}^{M} \left(t_{m,N}\phi_m(r) + s_{m,N}\varphi_m(r) + \psi_{m,N}(r)\right) e^{\mathrm{i}m\theta}$, where $\{t_{m,N}\}$ and $\{s_{m,N}\}$ are to be determined. Note that $\{\phi_{m,N}(r)\}$, $\{\varphi_{m,N}(r)\}$, and $\{\psi_{m,N}(r)\}$ can be efficiently and accurately computed (cf. [24, 31]). Therefore, the main challenge in finding u_{MN} lies in determining $\{t_{m,N}\}$ and $\{s_{m,N}\}$. In fact, it is straightforward to observe that the conditions required for the determination of $\{t_{m,N}\}$ and $\{s_{m,N}\}$ are derived from the boundary conditions

$$\left(u_{MN}, e^{\mathrm{i}k\theta}\right)_\Gamma = \left(g, e^{\mathrm{i}k\theta}\right)_\Gamma, \quad \left(\partial_r u_{MN}, e^{\mathrm{i}k\theta}\right)_\Gamma = \left(h, e^{\mathrm{i}k\theta}\right)_\Gamma \text{ for } |k| = 0, \cdots, M \tag{2.37}$$

which are equivalent to: for all $|k| = 0, 1, \cdots, M$,

$$\begin{aligned}
&\sum_{|m|=0}^{M} t_{m,N} \int_0^{2\pi} \phi_{m,N}(\rho(\theta)) e^{\mathrm{i}(m-k)\theta} \mathrm{d}\theta + \sum_{|m|=0}^{M} s_{m,N} \int_0^{2\pi} \varphi_{m,N}(\rho(\theta)) e^{\mathrm{i}(m-k)\theta} \mathrm{d}\theta \\
&\qquad = \int_0^{2\pi} g(\rho(\theta), \theta) e^{-\mathrm{i}k\theta} \mathrm{d}\theta - \sum_{|m|=0}^{M} \int_0^{2\pi} \psi_{m,N}(\rho(\theta)) e^{\mathrm{i}(m-k)\theta} \mathrm{d}\theta, \\
&\sum_{|m|=0}^{M} t_{m,N} \int_0^{2\pi} \partial_r \phi_{m,N}(\rho(\theta)) e^{\mathrm{i}(m-k)\theta} \mathrm{d}\theta + \sum_{|m|=0}^{M} s_{m,N} \int_0^{2\pi} \partial_r \varphi_{m,N}(\rho(\theta)) e^{\mathrm{i}(m-k)\theta} \mathrm{d}\theta \\
&\qquad = \int_0^{2\pi} h(\rho(\theta), \theta) e^{-\mathrm{i}k\theta} \mathrm{d}\theta - \sum_{|m|=0}^{M} \int_0^{2\pi} \partial_r \psi_{m,N}(\rho(\theta)) e^{\mathrm{i}(m-k)\theta} \mathrm{d}\theta.
\end{aligned} \tag{2.38}$$

Setting the discrete test space to be

$$Y_{MN} := \left\{ v_{MN}(r, \theta) = \sum_{|m|=0}^{M} v_{m,N}(r) e^{\mathrm{i}m\theta} \,\middle|\, v_{m,N} \in \hat{Y}_N^m \right\}, \tag{2.39}$$

then, the discrete Petrov-Galerkin formulation for (2.28) is given by

$$\begin{cases} \text{Find } u_{MN} \in X_{MN} \text{ such that} \\ \mathcal{A}(u_{MN}, v_{MN}) = (rf, v_{MN}), \quad \forall v_{MN} \in Y_{MN}. \end{cases} \tag{2.40}$$

Let $\phi_{m,N}(r)$, $\varphi_{m,N}(r)$, and $\psi_{m,N}(r)$ be the solutions of (2.32)-(2.34), respectively. And $\{t_{m,N}\}$ and $\{s_{m,N}\}$ are determined from (2.38). Then, it is easy to verify that

$$u_{MN}(r, \theta) = \sum_{|m|=0}^{M} u_{m,N}(r) e^{\mathrm{i}m\theta} \quad \text{with} \quad u_{m,N}(r) = t_{m,N}\phi_{m,N}(r) + s_{m,N}\varphi_{m,N}(r) + \psi_{m,N}(r) \tag{2.41}$$

is a solution of (2.40).

Hence, the main task is to determine $t_{m,N}$ and $s_{m,N}$.

2.4 Robust Algorithm for Solving Undetermined Coefficients

The linear system (2.38) for $t_{m,N}$ and $s_{m,N}$ is typically well-conditioned when Ω closely approximates a circle, i.e., $\rho(\theta) \approx \rho$, where ρ is a constant. However, for more complex geometries, the condition number of the matrix $\mathbf{A_L}$ of the linear system (2.38) tends to increase exponentially with M, as demonstrated numerically in Figure 2.

To address this issue, we propose an alternative approach. Specifically, we prescribe K equispaced sampling nodes $\{\hat{r}_k, \hat{\theta}_k\}_{k=1}^K$ on Γ, where $\hat{r}_k = \rho(\hat{\theta}_k)$, and enforce the following conditions:

$$\begin{aligned}
&\sum_{|m|=0}^{M} \left(t_{m,N}\phi_{m,N}(\hat{r}_k) + s_{m,N}\varphi_{m,N}(\hat{r}_k) + \psi_{m,N}(\hat{r}_k) \right) e^{\mathrm{i}m\hat{\theta}_k} = g(\hat{r}_k, \hat{\theta}_k), \quad k = 1, \ldots, K, \\
&\sum_{|m|=0}^{M} \partial_r \left(t_{m,N}\phi_{m,N}(\hat{r}_k) + s_{m,N}\varphi_{m,N}(\hat{r}_k) + \psi_{m,N}(\hat{r}_k) \right) e^{\mathrm{i}m\hat{\theta}_k} = h(\hat{r}_k, \hat{\theta}_k), \quad k = 1, \ldots, K.
\end{aligned} \tag{2.42}$$

When $K > 2M+1$, (2.42) is over determined and will be solved in the least squares sense, denoted as $\min_{\mathbf{t}} \|\mathbf{A}\mathbf{t} - \mathbf{b}\|_2$, by using standard numerical methods such as QR factorization or singular value decomposition (SVD).

However, when the sizes M and K increase, the collocation nodes $\{\hat{r}_k, \hat{\theta}_k\}_{k=1}^K$ become densely distributed, causing adjacent rows of the matrix $\mathbf{A}$ to be nearly parallel, leading to ill conditioning and compromising the stability and accuracy. To mitigate this issue, we consider two methods: truncated SVD and ridge regression.

The first method we propose is the truncated SVD, which is among the most widely used approaches for solving ill-conditioned linear systems. More precisely, by selecting a truncation number $\kappa > 0$, the approximate solution is given by

$$\mathbf{t}_\kappa = \sum_{i=1}^{\kappa} \left(\mathbf{u}_i^T \mathbf{b} / \sigma_i \right) \mathbf{v}_i, \tag{2.43}$$

where $\mathbf{U}^\top \mathbf{A}\mathbf{V} = \Sigma$ is the SVD of $\mathbf{A}$ with column partitions $\mathbf{U} = [\mathbf{u}_1, \ldots, \mathbf{u}_K]$, and $\sigma_1, \ldots, \sigma_\kappa$ are the κ largest singular values. In practice, we typically select κ to be the rank of $\mathbf{A}$, which helps to mitigate the effects of noise and numerical errors. Numerical experiments have shown that this choice can significantly enhance both the stability and accuracy of the solution.

The second method we recommend is ridge regression, also known as Tikhonov regularization. This method introduces a L^2 regularization term to the least squares objective function to stabilize the solution process. Specifically, we aim to minimize the objective function $\|\mathbf{A}\mathbf{r} - \mathbf{b}\|^2 + \lambda \|\mathbf{r}\|^2$, where $\lambda > 0$ is the regularization parameter. This can be reformulated as an augmented least squares problem:

$$\min_{\mathbf{r}} \left\| \begin{bmatrix} \mathbf{A} \\ \sqrt{\lambda}\mathbf{I} \end{bmatrix} \mathbf{r} - \begin{bmatrix} \mathbf{b} \\ 0 \end{bmatrix} \right\|^2 := \min_{\mathbf{r}} \|\mathbf{A}_{\mathbf{RR}}\mathbf{r} - \tilde{\mathbf{b}}\|^2. \tag{2.44}$$

In Figure 2, we present the condition numbers of the three matrices A_L, A and A_{RR} as M varies, using the complex domain defined in (3.2) and setting $K = 6M$ in the least squares formulation. In practical implementations, we empirically choose $\sqrt{\lambda} = O(10^{-7})$, which provides a good balance between conditioning and efficiency for the augmented least squares problem (2.44). This choice is based on extensive numerical experiments that demonstrate its effectiveness in stabilizing the solution process. This fixed value is used consistently throughout all numerical experiments in this work, demonstrating the robustness of the proposed method without the need for case-by-case parameter tuning. The numerical results indicate that as M increases, employing ridge regression to determine the undetermined coefficients becomes progressively more advantageous. These methods effectively stabilize the solution process and enhance the accuracy of the results.

In summary, we solve (2.40) using the following algorithm:

ALGORITHM 2.5 *Given M (degree of freedom in the θ direction) and N (degree of freedom in the r direction), we find an approximation to the extended problem (2.1) as follows:*

Step 1. Compute the truncated Fourier expansion of $f(r,\theta) := F(r\cos\theta, \sin\theta)$ with respect to θ, obtaining an approximation to (2.5).

Step 2. Compute $\{\phi_{m,N}\}$, $\{\varphi_{m,N}\}$, and $\{\psi_{m,N}\}$ which satisfy a sequence of 1-D fourth-order problems, using the spectral-Galerkin method described in [24, 30], following the homogenizations discussed in Remark 2.1.

Step 3. Choose a suitable $K > 2M+1$ and find $\{t_m\}$ and $\{s_m\}$ by solving the least squares problem corresponding to (2.42).

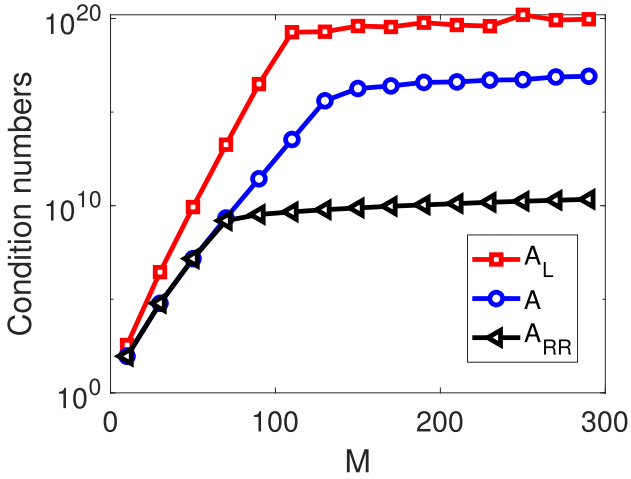

Fig. 2 Condition numbers of different matrices vs. M

Step 4. *Compute* $u_{MN}\left(r_k, \theta_j\right) = \sum_{|m|=0}^{M} u_{m,N}\left(r_k\right) e^{\mathrm{i}m\theta_j}$ *with*

$$u_{m,N}(r) = t_{m,N}\phi_{m,N}(r) + s_{m,N}\varphi_{m,N}(r) + \psi_{m,N}(r),$$

and obtain the final approximate solution $U_{MN}\left(x_{k,j}, y_{k,j}\right) = u_{MN}\left(\mathbb{T}^{-1}\left(x_{k,j}, y_{k,j}\right)\right)$ $(0 \le k \le N,\ 0 \le |j| \le M)$.

3 Numerical Results

We present in this section several numerical examples to demonstrate the effectiveness and flexibility of our algorithm. For all examples, we set $\alpha = 5$ and $\beta = 3$ in (1.1).

3.1 Accuracy Tests

To validate the effectiveness of the proposed method, we conducted a series of accuracy tests.

In the first example, we consider a smooth exact solution given by

$$U(x, y) = (x^2 - 2y^3 + 1)(\sin^2(2\pi(x^2 + y^2)) + x^3 + 1) \tag{3.1}$$

in a smooth domain (see Figure 3)

$$\Omega = \{(r, \theta) : r < 0.8 + 0.2\sin(4\theta)\}. \tag{3.2}$$

We approximate the undetermined coefficients $\{t_m\}$ and $\{s_m\}$ using the algorithm proposed in subsection 2.4. We set $N = 2M$ and plot the relative L^2 and L^∞ errors versus M in Figure 3. The results indicate that the errors decay exponentially as M increases. Table 1 lists the CPU times to validate the efficiency of our method. Specifically, T_{homo} refers to the time required for the initial two steps (solving the homogeneous boundary value problem), while T_{least} corresponds to the third step (solving the least squares problem). The results show that the overhead from the small-scale least squares problem is marginal, thereby confirming the overall computational effectiveness of the algorithm.

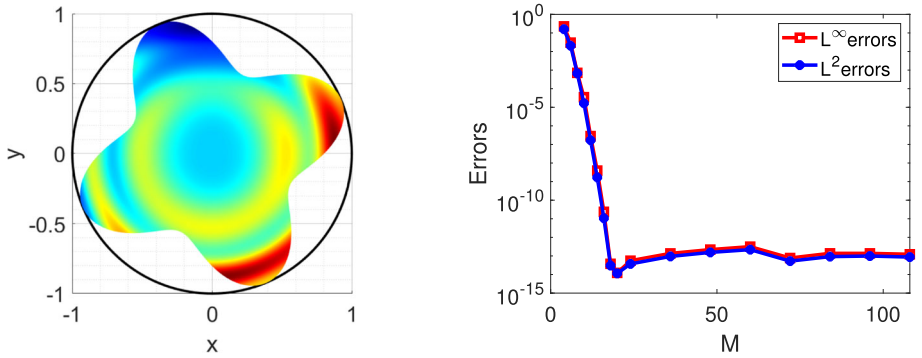

Fig. 3 The original domain (3.2) and the relative errors versus M in the first example

Table 1 CPU times (in seconds) for the first example

MN	4608	7200	10368	14112	18432	23328
T_{homo}	0.0277	0.0454	0.0580	0.0805	0.1101	0.1330
T_{least}	0.0039	0.0072	0.0110	0.0148	0.0229	0.0283

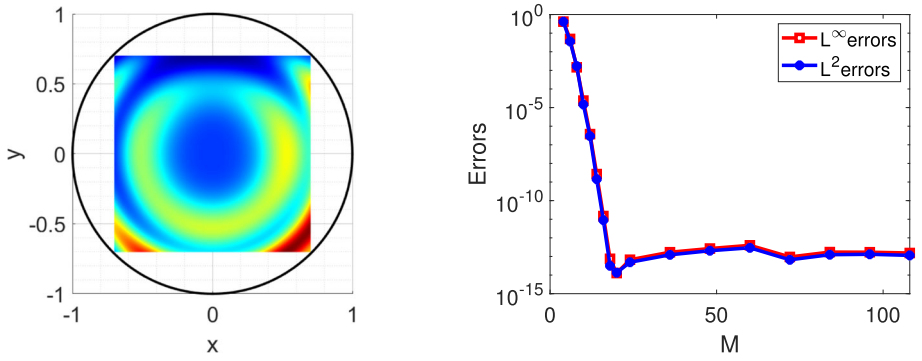

Fig. 4 The original square domain and the relative errors versus M in the second example

In the second example, we change the domain to a square (see Figure 4), while keeping the other settings the same as in the first example. The numerical results are shown in Figure 4. We also observe an exponential convergence rate, despite the fact that the domain is not smooth.

To further illustrate the advantages of our method in dealing with irregular regions, we consider two more complex non-smooth domains in the third example: a tear drop: $\Omega = \{(x, y) : (x + a)(x - a)^2 - (2a)^2 y^2 \geq 0,\ a = 1\}$, and a hexagon as shown in the first row of Figure 5. In the second row of Figure 5, we plot the relative L^2 and L^{∞} errors versus M. We also observe exponential convergence despite the non-smooth nature of the domains.

In the fourth example in this subsection, we consider an exact solution with limited regularity:

$$U(x, y) = (1 + (x^4 + y^4)^h) e^{\frac{y}{x+2}} \tag{3.3}$$

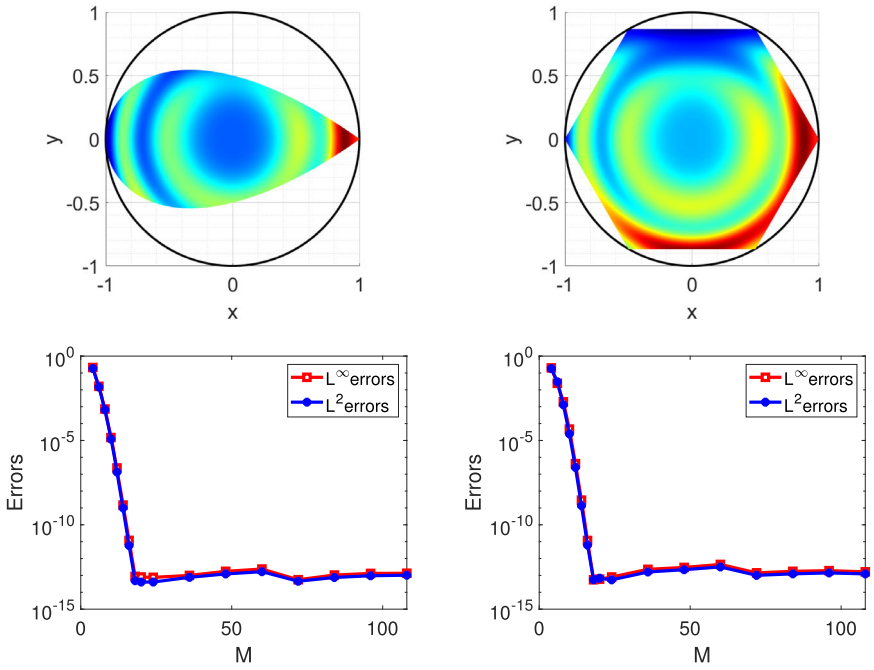

Fig. 5 Two complex non-smooth domains (upper): Tear drop (left) and Hexagon (right); and their relative errors versus M (lower) in the third example

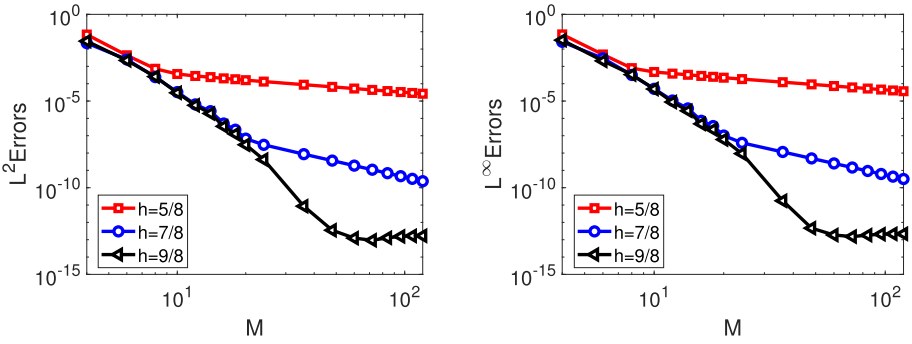

Fig. 6 The relative L^2 and L^∞ errors versus M for the low regularity test solution (3.3) in the fourth example

in a smooth domain given by (3.2). In Figure 6, we plot the relative L^2 and L^∞ errors versus M in log-log scale for different values of h. The results show an algebraic decay of the error with respect to M, with the convergence rate increasing for larger values of h.

The numerical results presented above indicate that our method achieves spectral accuracy, namely, the convergence rate only depends on the smoothness of the exact solution.

To conclude this subsection, we consider the homogeneous problem (1.1) (i.e., $F \equiv 0$) with $\alpha = \beta = 0$ on a non-convex domain, $\Omega = \{(r, \theta) : r < 0.8 + 0.2\sin(4\theta)\}$. Take the smooth boundary conditions $u|_{\partial\Omega} = \sin(x + y)$ and $\frac{\partial u}{\partial \mathbf{n}}|_{\partial\Omega} = \cos(x + y)$.

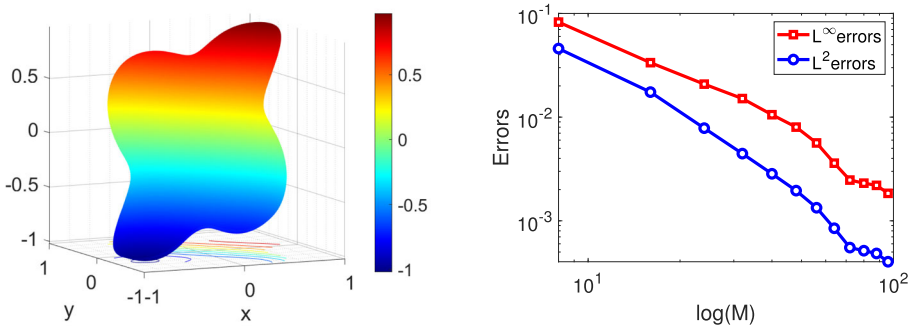

Fig. 7 The reference solution (left) and the relative errors versus M for the unknown solution (right) in the fifth example

A reference solution is computed with a fine discretization of $M = N = 256$ (Figure 7, left). The errors of less-resolved solutions are measured against this reference and are plotted versus M (Figure 7, right). The error curves exhibit linear trend on the log-log plot, which confirms the algebraic convergence of this singular solution.

3.2 Application to the Generalized Stokes Problem

As an important application in fluid mechanics, we consider the following generalized Stokes problem which arises after an implicit-explicit time discretization of the time dependent Navier-Stokes equations:

$$\begin{aligned} \gamma \mathbf{u} - \mu \Delta \mathbf{u} + \nabla p &= \mathbf{f}, \quad \text{in } \Omega, \\ \nabla \cdot \mathbf{u} &= 0, \quad \text{in } \Omega, \\ \mathbf{u} &= \mathbf{0}, \quad \text{on } \partial\Omega. \end{aligned} \tag{3.4}$$

It reduces to the standard Stokes problem when $\gamma = 0$.

A main challenge in solving the generalized Stokes problem (3.4) is the coupling between the velocity field $\mathbf{u}$ and the pressure p through the incompressibility constraint $\nabla \cdot \mathbf{u} = 0$.

In the two dimensional case, we can write $\mathbf{u} = \nabla \times \psi$ where ψ is the stream function. Then, applying the curl operator to the first equation in (3.4), and using $\mathbf{u} = \nabla \times \psi$, we obtain the following fourth-order problem for the stream function ψ:

$$\mu \Delta^2 \psi - \gamma \Delta \psi = \nabla \times \mathbf{f}, \tag{3.5}$$

$$\psi|_{\partial\Omega} = 0, \quad \frac{\partial \psi}{\partial \mathbf{n}}|_{\partial\Omega} = 0. \tag{3.6}$$

Consequently, the proposed algorithm can be employed for solving the above problem. Once we obtain the stream function ψ, we can easily obtain the velocity field through $\mathbf{u} = \nabla \times \psi$. Once the velocity $\mathbf{u}$ is known, the pressure can then be obtained by solving a pressure Poisson equation.

We now present some numerical examples for the generalized Stokes problem (3.4).

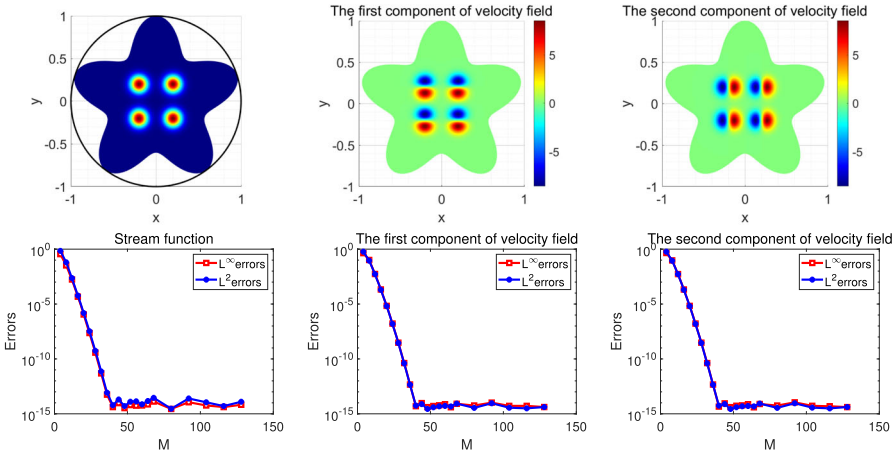

Fig. 8 The stream function, velocity field, and their convergence rates of accuracy test (3.7) for the generalized Stokes problem

We begin with an accuracy test. We set the viscosity $\mu = 1$ and $\gamma = 2000$, and the exact solution to be:

$$\psi(x, y) = \sum_{i=1}^{4} \exp(-100((x + x_i)^2 + (y + y_i)^2)), \quad |x_i| = |y_i| = 0.2, \tag{3.7}$$

defined in a smooth domain:

$$\Omega = \{(r, \theta) : r < 0.8 + 0.2 \sin(5\theta)\}. \tag{3.8}$$

The numerical results, as shown in Figure 8, demonstrate the exponential convergence of the algorithm. The accuracy of the computed stream function and velocity fields is validated against the analytical solution, confirming the robustness of our method in handling the generalized Stokes problem.

Next, we explore the application of our method in laser material processing, as discussed in [28]. The scenario involves various physical interactions, where the heated material can be modeled using viscous flow, specifically the Stokes equations. For this case, we focus solely on the fluid component, with the laser beam mathematically represented by a non-homogeneous right-hand side point force modeled as a smoothed Gaussian curve.

We consider the Stokes problem in the unit square domain $(0, 1)^2$ with the homogeneous Dirichlet boundary conditions. The dynamic viscosity is specified as $\mu = 0.0022$. The right-hand side $\mathbf{f}$ of (3.4) is defined as follows:

$$\mathbf{f} = \begin{pmatrix} f_1 \\ f_2 \end{pmatrix} = \begin{pmatrix} 0 \\ c_1 \exp(-c_2(\boldsymbol{x} - \boldsymbol{x}_0)^2) \end{pmatrix}, \quad \boldsymbol{x} \in \Omega, \tag{3.9}$$

with parameters $c_1 = 0.001$, $c_2 = 100$, and $\boldsymbol{x}_0 = (0.75, 0.75)$.

The numerically velocity fields are plotted in the second row of Figure 9. For comparison, we also plot, in the first row of Figure 9, the results obtained in [23]. It is evident that the results of our method align well with those reported in the literature.

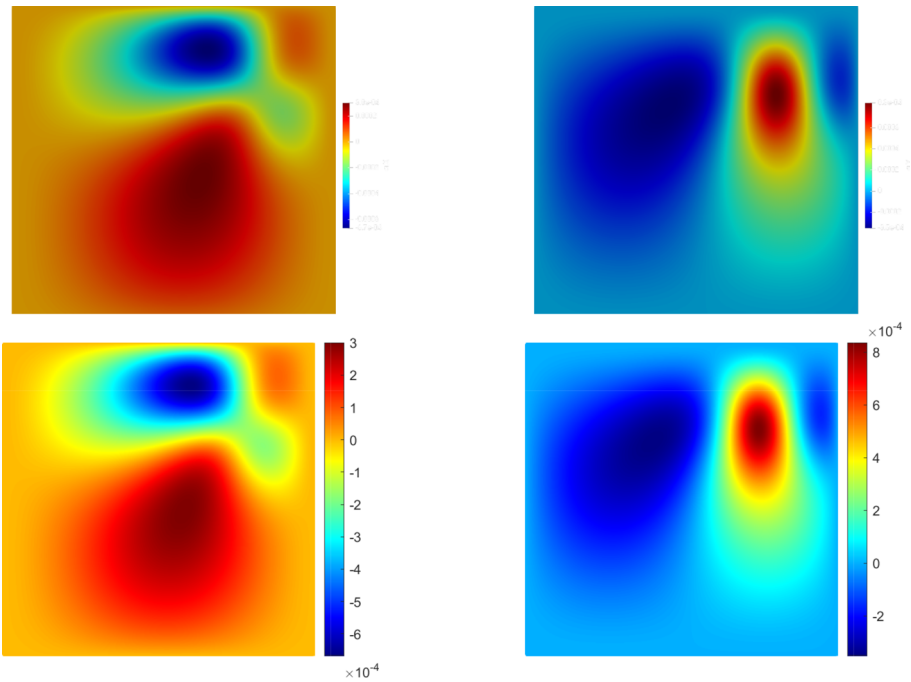

Fig. 9 Comparison of the velocity fields in laser beam material processing: reference (top) and ours (bottom)

4 The Fourth-Order Problems with Neumann Boundary Conditions

In this section, we consider the fourth-order problems with Neumann boundary conditions, which often arises in phase-field models. The general form is given by:

$$\begin{aligned} \alpha V - \beta \Delta V + \Delta^2 V &= F, && \text{in } \Omega, \\ \frac{\partial V}{\partial \mathbf{n}} &= G, && \text{on } \partial\Omega, \\ \frac{\partial \Delta V}{\partial \mathbf{n}} &= H, && \text{on } \partial\Omega. \end{aligned} \tag{4.1}$$

4.1 Direct Extension to Neumann Problems

While the preceding analysis focused on boundary conditions of the form (1.1), the proposed framework can be readily extended to the fourth-order Neumann problem (4.1).

Analogous to the previous section, we embed the complex geometry Ω into a disk $\tilde{\Omega}$ and consider the extended problem for a function U in $\tilde{\Omega}$:

$$\begin{aligned} \alpha U - \beta \Delta U + \Delta^2 U &= F, && \text{in } \tilde{\Omega}, \\ \frac{\partial U}{\partial \mathbf{n}} &= G, && \text{on } \partial\Omega, \\ \frac{\partial \Delta U}{\partial \mathbf{n}} &= H, && \text{on } \partial\Omega. \end{aligned} \tag{4.2}$$

By construction, any solution U to (4.2) satisfies $U|_\Omega = V$. Our goal is therefore to find a sufficiently smooth solution to this extended problem. The 2D problem is then reduced to a series of 1D problems via a polar coordinate transformation and Fourier series expansion, following the same procedure as in the previous section.

A key aspect of our approach is the introduction of undetermined coefficients corresponding to Dirichlet-type data, even though the original problem is posed with Neumann conditions:

$$u_m(1) = t_m, \quad \partial_r u_m(1) = s_m, \quad |m| = 0, 1, \dots \tag{4.3}$$

The justification for this choice lies in the well-posedness of the original problem. The existence of a unique solution implies that all associated quantities-including the solution's boundary values-are uniquely determined. Therefore, the parameterization of the solution, whether by its boundary values (t_m, s_m) or its normal derivatives, is a matter of representational convenience rather than fundamental necessity. The primary criterion is which parameterization most readily yields an explicit expression for the solution.

As in Section 2.1, we decompose the problem into three independent subproblems. The solution $u_m(r)$ can then be explicitly constructed as a linear combination of the solutions to these subproblems:

$$u_m(r; t_m, s_m) = t_m \phi_m(r) + s_m \varphi_m(r) + \psi_m(r), \tag{4.4}$$

where $\phi_m(r)$, $\varphi_m(r)$, and $\psi_m(r)$ are the solutions to the following problems, respectively:

$$\begin{aligned}
&\mathcal{L}_{\alpha,\beta,m}\phi_m(r) = 0, \quad \text{with} \quad \phi_m(1) = 1, \quad \partial_r\phi_m(1) = 0,\\
&\mathcal{L}_{\alpha,\beta,m}\varphi_m(r) = 0, \quad \text{with} \quad \varphi_m(1) = 0, \quad \partial_r\varphi_m(1) = 1,\\
&\mathcal{L}_{\alpha,\beta,m}\psi_m(r) = f_m(r), \quad \text{with} \quad \psi_m(1) = 0, \quad \partial_r\psi_m(1) = 0,
\end{aligned} \tag{4.5}$$

where $\mathcal{L}_{\alpha,\beta,m} = \alpha - \beta\mathcal{L}_m + \mathcal{L}_m^2$, and all solutions satisfy the requisite pole conditions from (2.7).

The undetermined coefficients $\{t_{m,N}\}$ and $\{s_{m,N}\}$ are found by enforcing the original Neumann boundary conditions at K equispaced collocation points $\{\hat{r}_k, \hat{\theta}_k\}_{k=1}^K$ on the boundary $\partial\Omega$. This leads to the least-squares system:

$$\begin{aligned}
&\sum_{|m|=0}^{M} \partial_r\Big(t_{m,N}\phi_{m,N}(\hat{r}_k) + s_{m,N}\varphi_{m,N}(\hat{r}_k) + \psi_{m,N}(\hat{r}_k)\Big)e^{\mathrm{i}m\hat{\theta}_k} = g(\hat{r}_k, \hat{\theta}_k), \quad k = 1, \dots, K,\\
&\sum_{|m|=0}^{M} \partial_r\Big(t_{m,N}\mathcal{L}_m\phi_{m,N}(\hat{r}_k) + s_{m,N}\mathcal{L}_m\varphi_{m,N}(\hat{r}_k) + \mathcal{L}_m\psi_{m,N}(\hat{r}_k)\Big)e^{\mathrm{i}m\hat{\theta}_k} = h(\hat{r}_k, \hat{\theta}_k), \quad k = 1, \dots, K.
\end{aligned} \tag{4.6}$$

We solve this system for $\{t_{m,N}, s_{m,N}\}$ using the robust algorithm described in Section 2.4.

The overall algorithm is essentially identical to the one previously described. The only difference lies in the final least-squares system (4.6), which is formulated based on the specific boundary conditions of the original problem. This flexibility highlights the generality of our framework. However, this generality is not without cost. A potential drawback is a loss of accuracy for certain problems. The case under consideration exemplifies this trade-off, as enforcing the condition on $\partial_r(\Delta V)$ requires evaluating third-order derivatives of the solution basis functions, which can be a numerically sensitive operation.

We now present a numerical example to illustrate the accuracy of the proposed scheme. We consider problem (4.1) with $\alpha = 5$, $\beta = 3$ and an exact solution given by

$$V(x, y) = (x^2 - 2y + 1)\exp(x - y) \tag{4.7}$$

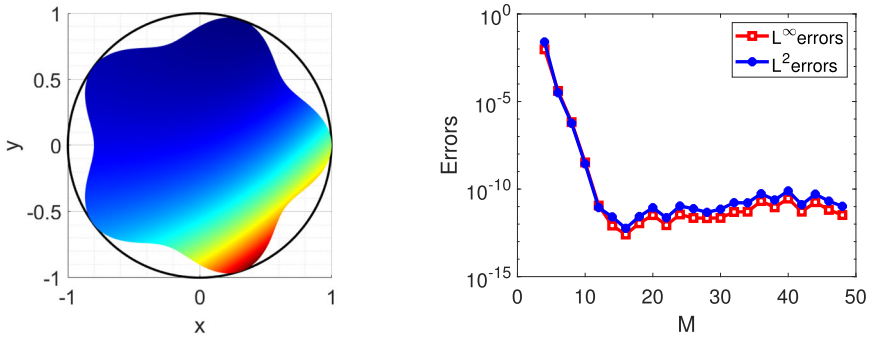

Fig. 10 The original domain (4.8) and the relative errors versus M

in a smooth domain (see Figure 10)

$$\Omega = \{(r, \theta) : r < 0.9 + 0.1\cos(5\theta)\}. \tag{4.8}$$

We set $N = 2M$ and plot the relative L^2 and L^∞ errors versus M in Figure 10. We observe exponential decay of the errors as M increases, indicating the versatility and robustness of our proposed framework.

4.2 An Alternative Approach via a Second-Order System

In many cases such as in phase-field models, a fourth-order problem (4.1) is often reformulated as a coupled second-order equations. Hence, we present an alternative approach that proceeds in three stages: reformulating the fourth-order equation as a second-order system, embedding the problem in a regular domain, and constructing a new decomposition for the solution.

First, we introduce an auxiliary function $\tilde{V} = -\Delta V + \epsilon V$ with a constant $\epsilon > 0$. By substituting this into the original problem (4.1), we derive an equivalent second-order coupled system:

$$\begin{aligned} -\Delta\tilde{V} + (\beta - \epsilon)\tilde{V} + \left(\epsilon^2 - \epsilon\beta + \alpha\right) V &= F, && \text{in } \Omega, \\ -\Delta V + \epsilon V - \tilde{V} &= 0, && \text{in } \Omega, \\ \frac{\partial V}{\partial \mathbf{n}} &= G, && \text{on } \partial\Omega, \\ \frac{\partial \tilde{V}}{\partial \mathbf{n}} &= -H + \epsilon G, && \text{on } \partial\Omega. \end{aligned} \tag{4.9}$$

Next, following the same embedding procedure as before, we extend the problem from the complex domain Ω to a disk $\tilde{\Omega}$. This yields an extended system for the functions U and W in $\tilde{\Omega}$ which, by construction, satisfy $U|_\Omega = V$ and $W|_\Omega = \tilde{V}$. Applying a Fourier transform in the angular direction reduces the 2D system to a sequence of 1D coupled boundary value problems for the Fourier coefficients $u_m(r)$ and $w_m(r)$.

To solve these 1D problems, we devise below a new decomposition strategy. Let

$$u_m(1) = t_m, \quad w_m(1) = s_m, \quad |m| = 0, 1, \ldots \tag{4.10}$$

where the constants $\{t_m\}$ and $\{s_m\}$ are to be determined. Then, the solution pair (u_m, w_m) can be expressed as a linear combination of solutions to three independent subproblems:

$$\begin{aligned} u_m(r; t_m, s_m) &= u_m^1(r) + t_m u_m^2(r) + s_m u_m^3(r), \\ w_m(r; t_m, s_m) &= w_m^1(r) + t_m w_m^2(r) + s_m w_m^3(r), \end{aligned} \tag{4.11}$$

where the pairs $(u_m^1, w_m^1)^T$, $(u_m^2, w_m^2)^T$, and $(u_m^3, w_m^3)^T$ solve three separate systems, each being a second-order coupled ODE with homogeneous Dirichlet boundary conditions and appropriate pole conditions. More specifically, $\left(u_m^1(r), w_m^1(r)\right)^T$ is the solution of

$$\begin{aligned} -\mathcal{L}_m w_m^1(r) + (\beta - \epsilon) w_m^1(r) + \left(\epsilon^2 - \epsilon\beta + \alpha\right) u_m^1(r) &= f_m(r), \qquad 0 < r < 1, \\ -\mathcal{L}_m u_m^1(r) + \epsilon u_m^1(r) - w_m^1(r) &= 0, \qquad 0 < r < 1, \\ u_m^1(0) = 0 \ (m \neq 0), \quad u_m^1(1) &= 0, \\ w_m^1(0) = 0 \ (m \neq 0), \quad w_m^1(1) &= 0, \end{aligned} \tag{4.12}$$

$\left(u_m^2(r), w_m^2(r)\right)^T$ is the solution of

$$\begin{aligned} -\mathcal{L}_m w_m^2(r) + (\beta - \epsilon) w_m^2(r) + \left(\epsilon^2 - \epsilon\beta + \alpha\right) u_m^2(r) &= 0, \qquad 0 < r < 1, \\ -\mathcal{L}_m u_m^2(r) + \epsilon u_m^2(r) - w_m^2(r) &= 0, \qquad 0 < r < 1, \\ u_m^2(0) = 0 \ (m \neq 0), \quad u_m^2(1) &= 1, \\ w_m^2(0) = 0 \ (m \neq 0), \quad w_m^2(1) &= 0, \end{aligned} \tag{4.13}$$

and $\left(u_m^3(r), w_m^3(r)\right)^T$ is the solution of

$$\begin{aligned} -\mathcal{L}_m w_m^3(r) + (\beta - \epsilon) w_m^3(r) + \left(\epsilon^2 - \epsilon\beta + \alpha\right) u_m^3(r) &= 0, \qquad 0 < r < 1, \\ -\mathcal{L}_m u_m^3(r) + \epsilon u_m^3(r) - w_m^3(r) &= 0, \qquad 0 < r < 1, \\ u_m^3(0) = 0 \ (m \neq 0), \quad u_m^3(1) &= 0, \\ w_m^3(0) = 0 \ (m \neq 0), \quad w_m^3(1) &= 1. \end{aligned} \tag{4.14}$$

These decoupled systems, which feature homogeneous boundary conditions, can be solved efficiently using a spectral-Galerkin approach with appropriate basis functions [30, 31].

Finally, the undetermined coefficients $\{t_{m,N}\}$ and $\{s_{m,N}\}$ are found by enforcing the original Neumann boundary conditions (4.9) in a least-squares sense at K collocation points on the boundary Γ:

$$\begin{aligned} \sum_{|m|=0}^{M} \partial_r \left(t_{m,N} u_{m,N}^2(\hat{r}_k) + s_{m,N} u_{m,N}^3(\hat{r}_k) + u_{m,N}^1(\hat{r}_k) \right) e^{\mathrm{i}m\hat{\theta}_k} &= g(\hat{r}_k, \hat{\theta}_k), \\ \sum_{|m|=0}^{M} \partial_r \left(t_{m,N} w_{m,N}^2(\hat{r}_k) + s_{m,N} w_{m,N}^3(\hat{r}_k) + w_{m,N}^1(\hat{r}_k) \right) e^{\mathrm{i}m\hat{\theta}_k} &= -h(\hat{r}_k, \hat{\theta}_k) + \epsilon g(\hat{r}_k, \hat{\theta}_k). \end{aligned} \tag{4.15}$$

We solve this system using the robust algorithm from Section 2.4.

In terms of implementation, this method closely mirrors the previous one. The primary difference is that the direct approach solves fourth-order ODEs, whereas this alternative approach solves systems of second-order ODEs. This reduction in differential order, however, comes at the expense of generality. The second method is tailored to the specific Neumann

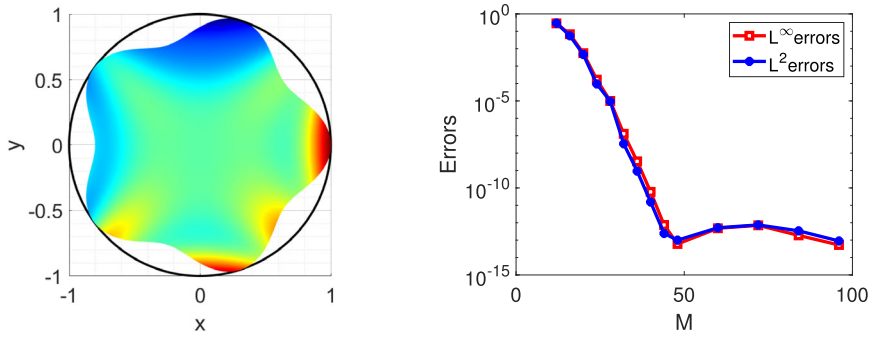

Fig. 11 The original domain and the relative errors versus M

boundary conditions in (4.1), while the first method can accommodate more general boundary conditions.

We now present a numerical example to validate the accuracy and effectiveness of this scheme. We consider a smooth exact solution

$$V(x, y) = (x^2 - 2y^3 + 1)(\cos^2(\pi(x^2 - y^2)) + x^3 + 1) \tag{4.16}$$

in the domain $\Omega = \{(r, \theta) : r < 0.9 + 0.1\cos(5\theta)\}$ (Figure 11). We set $N = 2M$ and $\alpha = 5$, $\beta = \epsilon = 3$. The relative L^2 and L^∞ errors, plotted against M in Figure 11, decay exponentially. The results confirm that for this class of problems, the second-order system approach is both highly accurate and efficient.

4.3 Application to the Cahn–Hilliard Equation

In this subsection, we focus on the Cahn–Hilliard equation [8], a widely-used phase-field model for binary mixtures, which is given with a source term by:

$$\begin{aligned} \frac{\partial u}{\partial t} &= \mathcal{M}\Delta\mu + F(x, y, t), \quad (x, y) \in \Omega, \quad t \in (0, T], \\ \mu &= -\Delta u + \frac{1}{\varepsilon^2}\mathcal{F}'(u), \quad (x, y) \in \Omega, \quad t \in (0, T], \end{aligned} \tag{4.17}$$

where $u(x, y, t)$ represents the concentration of one component in a binary alloy, Ω is a bounded domain in $\mathbb{R}^2$, and T is the final time. In the above system, $\mathcal{M} > 0$ represents a mobility constant. The parameter ε measures the interfacial thickness, which is small relative to the macroscopic length scale of the domain. The nonlinear term $\mathcal{F}'(u)$ is the derivative of the Ginzburg-Landau double-well potential, $\mathcal{F}(u) = \frac{1}{4}(u^2 - 1)^2$. To enhance the numerical stability of the scheme, we follow the common practice of using a truncated potential [10, 33]. The source term $F(x, y, t)$ is included only for the convergence study and is set to zero in physical simulations. We consider boundary conditions corresponding to a neutral wall on $\partial\Omega$ [39, 44]:

$$\begin{aligned} \mathbf{n} \cdot \nabla u &= G(x, y, t), \quad \text{on } \partial\Omega, \\ \mathbf{n} \cdot \nabla \mu &= H(x, y, t), \quad \text{on } \partial\Omega, \end{aligned} \tag{4.18}$$

where $\mathbf{n}$ is the outward-pointing unit normal vector to $\partial\Omega$. Similar to F, the terms G and H are non-zero only for the convergence test. The system is supplemented with the initial

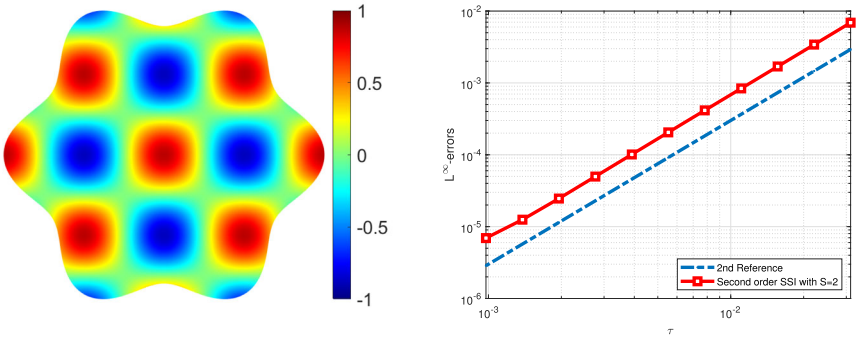

Fig. 12 Numerical solution at $T = 0.5$ (left) and its convergence rate (right)

condition:

$$u(x, y, 0) = u_0(x, y), \tag{4.19}$$

where $u_0(x, y)$ is the initial phase distribution.

For the temporal discretization, we employ the stabilized semi-implicit (SSI) schemes from [33] for their simplicity and effectiveness. We note, however, that more advanced structure-preserving methods are available, as reviewed in [35]. We consider a second-order scheme based on the generalized BDF2, which offers better stability than the usual BDF2, proposed in [21]:

$$\begin{aligned} \frac{(2\kappa+1)u^{n+1} - 4\kappa u^n + (2\kappa-1)u^{n-1}}{2\tau} &= \mathcal{M}\Delta\mu^{n+\kappa}, \\ -\Delta\hat{u}^{n+\kappa} + \frac{1}{\varepsilon^2}\mathcal{F}'\left((\kappa+1)u^n - \kappa u^{n-1}\right) + \frac{S}{\varepsilon^2}\left(\hat{u}^{n+\kappa} - (\kappa+1)u^n + \kappa u^{n-1}\right) &= \mu^{n+\kappa}, \end{aligned} \tag{4.20}$$

where

$$\hat{u}^{n+\kappa} := \kappa u^{n+1} - (\kappa-1)u^n. \tag{4.21}$$

The stabilization term adds a consistency error of order $\mathcal{O}(\frac{S\tau^2}{\varepsilon^2})$, which is of the same order as the extrapolation error. At each time step, the resulting system of PDEs is solved spatially using the method from Subsection 4.2, with the minor modification that the zero right-hand side of the second equation in the first subproblem, cf. (4.12), is replaced by the explicit terms from the time discretization.

We first verify the convergence rate of our scheme with $\kappa = 2$. We construct an exact solution $u(x, y, t) = \cos(2\pi x)\cos(2\pi y)\cos(t)$ by choosing suitable source and boundary terms. The computational domain is a smooth, flower-shaped region defined by $\Omega = \{(r, \theta) : r < 0.9 + 0.1\cos(6\theta)\}$. We set the spatial resolution to $N = M = 128$ to ensure the error is dominated by the temporal discretization. With parameters $T = 0.5$, $S = 2$, $\varepsilon = 0.5$, $\mathcal{M} = 0.1$, we plot the L^∞ errors against the time step size in Figure 12. The results clearly demonstrate the expected second-order accuracy in time.

To demonstrate the capability of our method for simulating complex interfacial dynamics of the Cahn–Hilliard equation, we next consider four problems, including some benchmark problems: the evolution of a single drop and the coalescence of two drops. Unless otherwise specified, we consider the non-dimensional parameters $\mathcal{M} = 5 \times 10^{-4}$, $\varepsilon = 0.008$, and the scheme with $N = M = 200$, $\delta t = 1 \times 10^{-3}$, $S = 2$, $\kappa = 2$.

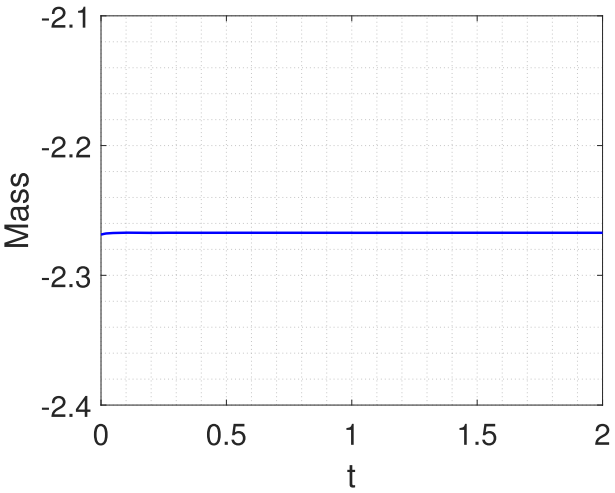

Fig. 13 Evolutions of mass in the Cahn–Hilliard equation (4.17) with initial condition (4.22)

Evolution of a single drop. We first simulate the evolution of a square drop in the smooth domain $\Omega = \{(r, \theta) : r < 0.9 + 0.1\cos(6\theta)\}$ with $u = \pm 1$ representing the two bulk materials. At $t = 0$, one material is located in a smaller square region with dimension $2h_0 \times 2h_0$ around the center of the domain, with the second material filling the remainder of the domain. The initial condition is given by

$$u_0(x, y) = \frac{1}{2}\Big(\tanh\frac{x + h_0}{\eta} - \tanh\frac{x - h_0}{\eta}\Big)\Big(\tanh\frac{y + h_0}{\eta} - \tanh\frac{y - h_0}{\eta}\Big) - 1. \quad (4.22)$$

We take $\eta = 0.01$, $h_0 = 0.25$ and solve the Cahn-Hilliard equation (4.17) with $F = 0$ and homogeneous Neumann boundary conditions ($G = H = 0$).

Figure 14 displays a temporal sequence of snapshots from the simulation. The initial square drop gradually evolves into a circle, as expected from the Cahn-Hilliard dynamics. In Figure 13, we plot the evolution of the total mass $\int_\Omega u(x, y, t)\mathrm{d}x\mathrm{d}y$.

Coalescence of two drops. Secondly, we simulate the coalescence of two drops within the same computational domain. The simulation starts with a different initial condition where one material occupies two adjacent circular regions:

$$u_0(x, y) = 1 - \tanh\frac{|\boldsymbol{x} - \boldsymbol{x}_0| - R_0}{\sqrt{2}\eta} - \tanh\frac{|\boldsymbol{x} - \boldsymbol{x}_1| - R_0}{\sqrt{2}\eta}, \quad (4.23)$$

where the centers are $\boldsymbol{x}_0 = (-0.2, 0)$ and $\boldsymbol{x}_1 = (0.2, 0)$, and the radius is $R_0 = 0.19$. We consider $\eta = 0.01$.

The coalescence process is shown in Figure 15. This merging is driven by the system's tendency to minimize its total interfacial free energy, since a single large drop has less surface area than two smaller drops of the same total volume. Once the drops make contact, surface tension acts to eliminate the high-curvature neck that forms between them, rapidly pulling the two masses into a single body. The two drops ultimately merge and evolve into a single circular drop, demonstrating the ability of our scheme to accurately capture such topological changes.

Influences of Neumann boundary conditions and complex geometry. Next, to investigate the influences of homogeneous Neumann boundary conditions and complex geometry,

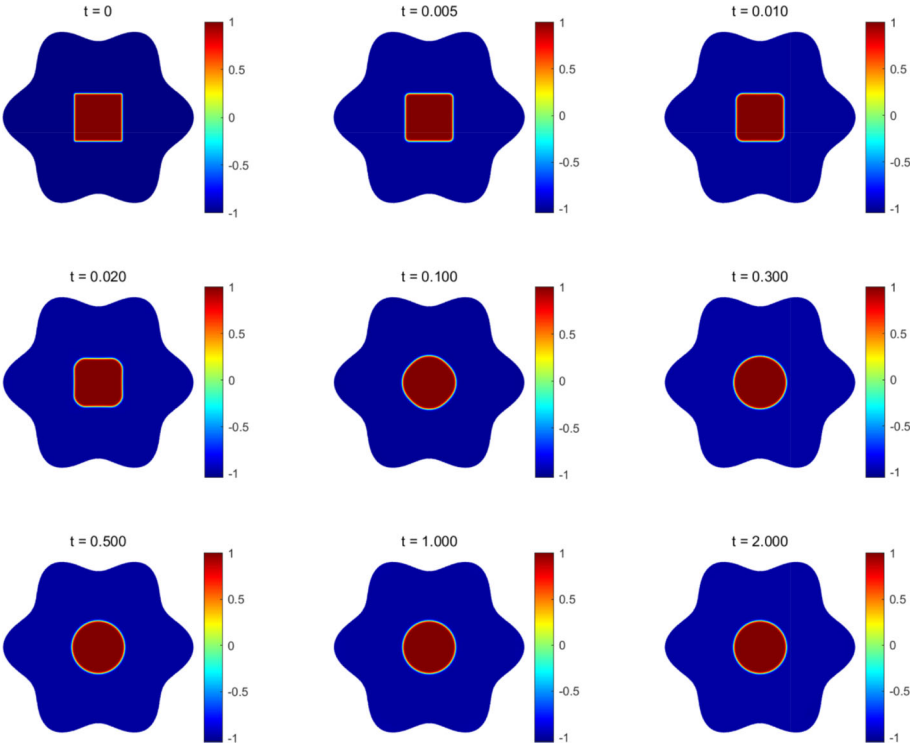

Fig. 14 Temporal sequence of snapshots showing the evolution of a drop with initial condition (4.22)

we consider an initial state where two drops are in contact with the domain boundary. We simulate the same two-drop coalescence but with an initial condition placing the drops in contact with the domain wall:

$$u_0(x, y) = 1 - \tanh \frac{|\boldsymbol{x} - \boldsymbol{x}_0| - R_0}{\sqrt{2}\eta} - \tanh \frac{|\boldsymbol{x} - \boldsymbol{x}_1| - R_0}{\sqrt{2}\eta}, \tag{4.24}$$

where the centers are now $\boldsymbol{x}_0 = (0.2, 0.5)$ and $\boldsymbol{x}_1 = (0.6, 0.5)$.

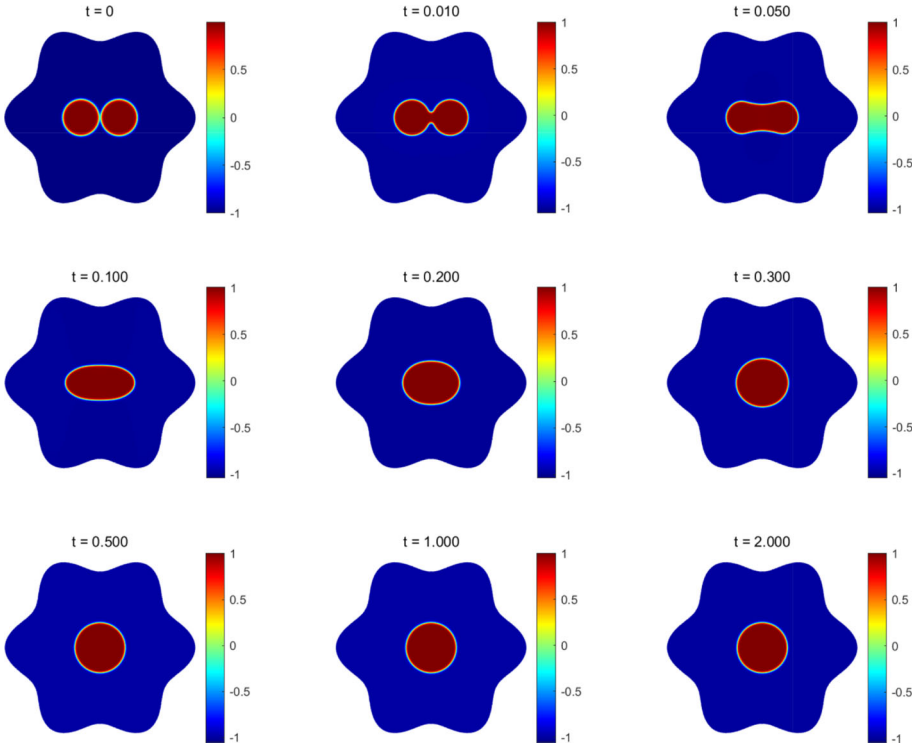

Fig. 15 Temporal sequence of snapshots showing the coalescence of two circular drops with initial condition (4.23)

Figure 16 illustrates how homogeneous Neumann boundary conditions, which enforce a 90-degree contact angle, interact with a complex geometry. Unlike in bulk or periodic systems, this contact angle requirement induces an attractive force that, when guided by the domain's curvature, drives the two drops to migrate and coalesce along the boundary. The final equilibrium state is a single semi-circular drop conforming to the wall. This example demonstrates robustness of our method in capturing the complex interplay between surface tension and geometric constraints.

Phase separation. Finally, we consider the spinodal decomposition of a homogeneous mixture into two coexisting phases governed by the Cahn–Hilliard equation in the same complex domain. The initial condition is a small random perturbation around a zero mean:

$$u_0(x, y) = 0.003 \times \big(2 \cdot \text{rand}(x, y) - 1\big), \tag{4.25}$$

where $rand(\,)$ generates uniformly distributed random numbers in $[0, 1]$. We set $\mathcal{M} = 0.001$, $\varepsilon = 0.006$ and $M = N = 300$.

Figure 17 shows the typical evolution process of the mixture. It can be observed that two phases separate from the initially homogeneous distribution of the mixture.

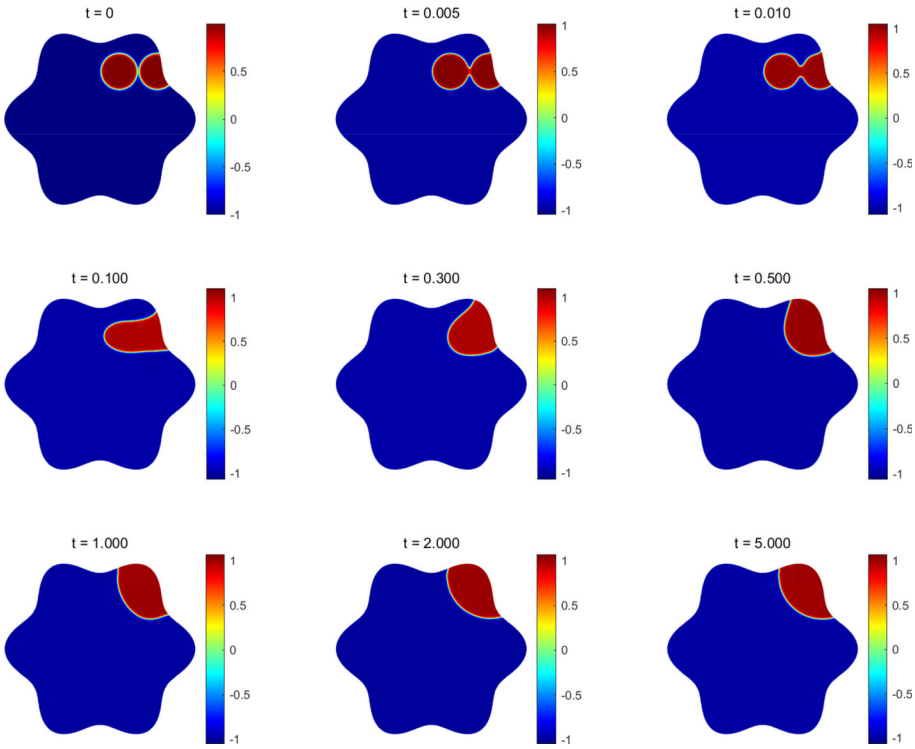

Fig. 16 Temporal sequence of snapshots showing the effect of boundary interaction with initial condition (4.24)

5 Concluding Remarks

We proposed in this paper an effective spectral method for solving fourth-order problems in two dimensional complex domains. By utilizing the circular embedding approach, the original two-dimensional problem is decomposed into a sequence of one-dimensional fourth-order problems with constant coefficients, plus a least squares problem to enforce the boundary conditions. The one-dimensional fourth-order problems can be efficiently solved using the standard spectral-Galerkin method, while the least squares problem can be accurately and stably solved by using a Tikhonov regularization technique. This algorithm demonstrates significant advantages in terms of efficiency and ease of implementation compared to the mapping approach. We presented ample numerical results which demonstrate that our algorithm achieves exponential convergence if the solution of the original problem is smooth.

We validated the robustness and broad applicability of our framework through two applications: the generalized Stokes problem and the Cahn-Hilliard equation. In both cases, our numerical simulations accurately captured the essential physical behaviors of the systems. This work not only extends the operational range of the circular domain embedding method to fourth-order problems but also affirms its significant promise for future research and development.

The method introduced in this paper can also be adapted to other complex geometries, such as exterior domains. Future research will focus on performing rigorous analyses for general

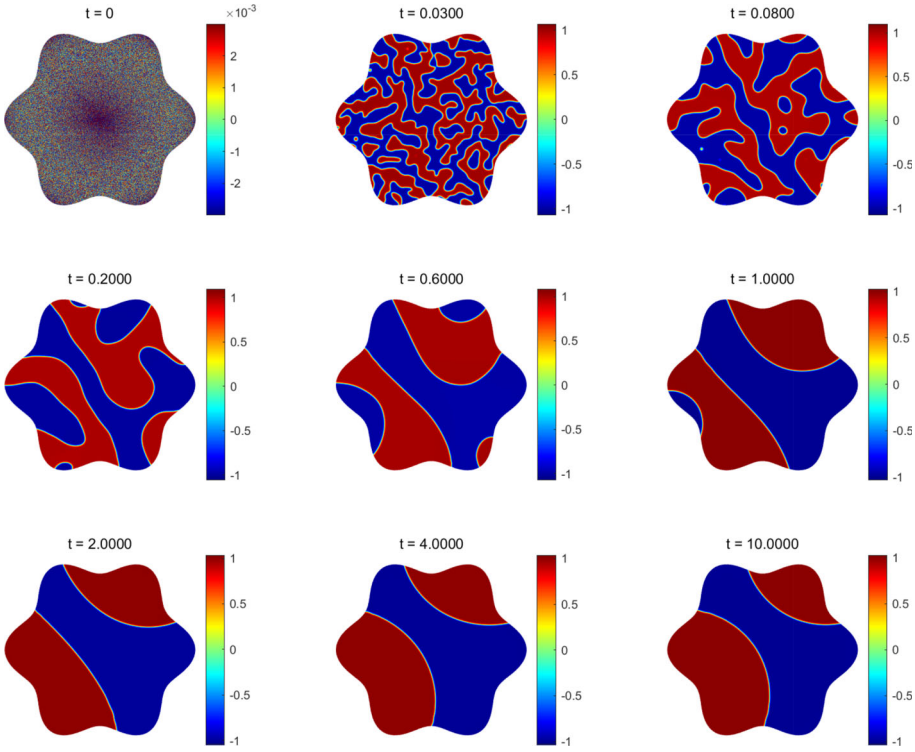

Fig. 17 Temporal sequence of snapshots showing the phase separation with random initial condition (4.25)

domains and exploring the applicability of this approach to more complicated problems, including the Navier-Stokes equations and other gradient flows.

Acknowledgements This work is supported in part by the National Natural Science Foundation of China through grants W2431008 and 12371409.

Author Contributions All authors contributed equally to prepare this manuscript. All authors read and approved the final manuscript.

Data Availability The data used to support the findings of this study are available from the corresponding author upon request.

Declarations

Conflicts of Interest The authors declare that they have no conflict of interest.

References

1. Adcock, B., Huybrechs, D., Martín-Vaquero, J.: On the numerical stability of Fourier extensions. Found. Comput. Math. **14**, 635–687 (2014). https://doi.org/10.1007/s10208-013-9158-8
2. Albin, N., Bruno, O.P., Cheung, T.Y., Cleveland, R.O.: Fourier continuation methods for high-fidelity simulation of nonlinear acoustic beams. J. Acoust. Soc. Am. **132**, 2371–2387 (2012). https://doi.org/10.1121/1.4742722

3. An, J., Li, H.Y., Zhang, Z.M.: Spectral-Galerkin approximation and optimal error estimate for biharmonic eigenvalue problems in circular/spherical/elliptical domains. Numer. Algorithms **84**, 427–455 (2020). https://doi.org/10.1007/s11075-019-00760-4
4. Angot, P., Bruneau, C.H., Fabrie, P.: A penalization method to take into account obstacles in incompressible viscous flows. Numer. Math. **81**, 497–520 (1999). https://doi.org/10.1007/s002110050401
5. Bialecki, B., Karageorghis, A.: A Legendre spectral Galerkin method for the biharmonic Dirichlet problem. SIAM J. Sci. Comput. **22**, 1549–1569 (2000). https://doi.org/10.1137/S1064827598342407
6. Boyd, JP.: *Chebyshev and Fourier spectral methods*, Dover Publications, Inc., Mineola, NY, second ed., (2001)
7. Buzbee, B.L., Dorr, F.W., George, J.A., Golub, G.H.: The direct solution of the discrete Poisson equation on irregular regions. SIAM J. Numer. Anal. **8**, 722–736 (1971). https://doi.org/10.1137/0708066
8. Cahn, J.W., Hilliard, J.E.: Free energy of a nonuniform system. I. Interfacial free energy. J. Chem. Phys. **28**, 258–267 (1958). https://doi.org/10.1063/1.1744102
9. Canuto, C., Hussaini, M.Y., Quarteroni, A., Zang, T.A.: Spectral methods: Evolution to complex geometries and applications to fluid dynamics. Scientific Computation, Springer, Berlin (2007)
10. Condette, N., Melcher, C., Süli, E.: Spectral approximation of pattern-forming nonlinear evolution equations with double-well potentials of quadratic growth. Math. Comp. **80**, 205–223 (2011). https://doi.org/10.1090/S0025-5718-10-02365-3
11. Dinh, Q.V., Glowinski, R., He, J., Kwock, V., Pan, T.W., Périaux, J.: *Lagrange multiplier approach to fictitious domain methods: application to fluid dynamics and electromagnetics*, in Fifth International Symposium on Domain Decomposition Methods for Partial Differential Equations (Norfolk, VA, 1991), SIAM, Philadelphia, PA, (1992) 151–194
12. Engel, G., Garikipati, K., Hughes, T.J.R., Larson, M.G., Mazzei, L., Taylor, R.L.: Continuous/discontinuous finite element approximations of fourth-order elliptic problems in structural and continuum mechanics with applications to thin beams and plates, and strain gradient elasticity. Comput. Methods Appl. Mech. Engrg. **191**, 3669–3750 (2002). https://doi.org/10.1016/S0045-7825(02)00286-4
13. Gopal, A., Trefethen, L.N.: New Laplace and Helmholtz solvers. Proc. Natl. Acad. Sci. **116**, 10223–10225 (2019)
14. Gopal, A., Trefethen, L.N.: Solving Laplace problems with corner singularities via rational functions. SIAM J. Numer. Anal. **57**, 2074–2094 (2019). https://doi.org/10.1137/19M125947X
15. Gordon, W.J., Hall, C.A.: *Transfinite element methods: blending-function interpolation over arbitrary curved element domains*, Numer. Math., 21 (1973/74) 109–129, https://doi.org/10.1007/BF01436298
16. Gu, Y.Q., Shen, J.: Accurate and efficient spectral methods for elliptic PDEs in complex domains. J. Sci. Comput. **83**(42), 20 (2020). https://doi.org/10.1007/s10915-020-01226-9
17. Gu, Y.Q., Shen, J.: An efficient spectral method for elliptic PDEs in complex domains with circular embedding. SIAM J. Sci. Comput. **43**, A309–A329 (2021). https://doi.org/10.1137/20M1345153
18. Gu, Y.Q., Shen, J.: A fictitious domain spectral method for solving the Helmholtz equation in exterior domains. J. Sci. Comput. **94**(46), 27 (2023). https://doi.org/10.1007/s10915-023-02098-5
19. Guo, B.Y.: *Spectral methods and their applications*, World Scientific Publishing Co., Inc., River Edge, NJ, (1998) https://doi.org/10.1142/9789812816641
20. Guo, B.Y., Wang, Z.Q., Wan, Z.S., Chu, D.L.: Second order Jacobi approximation with applications to fourth-order differential equations. Appl. Numer. Math. **55**, 480–502 (2005). https://doi.org/10.1016/j.apnum.2005.01.002
21. Huang, F.K., Shen, J.: On a new class of BDF and IMEX schemes for parabolic type equations. SIAM J. Numer. Anal. **62**, 1609–1637 (2024). https://doi.org/10.1137/23M1612986
22. Huybrechs, D.: On the Fourier extension of nonperiodic functions. SIAM J. Numer. Anal. **47**, 4326–4355 (2010). https://doi.org/10.1137/090752456
23. Jodlbauer, D., Langer, U., Wick, T., Zulehner, W.: Matrix-free monolithic multigrid methods for Stokes and generalized Stokes problems. SIAM J. Sci. Comput. **46**, A1599–A1627 (2024). https://doi.org/10.1137/22M1504184
24. Li, L., An, J.: An efficient spectral method and rigorous error analysis based on dimension reduction scheme for fourth order problems. Numer. Methods Partial Differential Equations **37**, 152–171 (2021). https://doi.org/10.1002/num.22523
25. Liu, F.J., Li, H.Y., Wang, Z.Q.: Spectral methods using generalized Laguerre functions for second and fourth order problems. Numer. Algorithms **75**, 1005–1040 (2017). https://doi.org/10.1007/s11075-016-0228-2
26. Lyon, M., Bruno, O.P.: High-order unconditionally stable FC-AD solvers for general smooth domains. II. Elliptic, parabolic and hyperbolic PDEs; theoretical considerations. J. Comput. Phys. **229**, 3358–3381 (2010). https://doi.org/10.1016/j.jcp.2010.01.006

27. Orszag, S.A.: Spectral methods for problems in complex geometries. J. Comput. Phys. **37**, 70–92 (1980). https://doi.org/10.1016/0021-9991(80)90005-4
28. Otto, A., Schmidt, M.: Towards a universal numerical simulation model for laser material processing. Phys. Procedia **5**, 35–46 (2010). https://doi.org/10.1016/j.phpro.2010.08.120
29. Quarteroni, A., Valli, A.: *Domain decomposition methods for partial differential equations*, Numerical Mathematics and Scientific Computation, The Clarendon Press, Oxford University Press, New York, Oxford Science Publications (1999)
30. Shen, J.: Efficient spectral-Galerkin method. I. Direct solvers of second- and fourth-order equations using Legendre polynomials. SIAM J. Sci. Comput. **15**, 1489–1505 (1994). https://doi.org/10.1137/0915089
31. Shen, J.: Efficient spectral-Galerkin methods. III. Polar and cylindrical geometries. SIAM J. Sci. Comput. **18**, 1583–1604 (1997). https://doi.org/10.1137/S1064827595295301
32. Shen, J., Tang, T., Wang, L.L.: *Spectral methods: Algorithms, analysis and applications*, vol. 41 of Springer Series in Computational Mathematics, Springer, Heidelberg, (2011) https://doi.org/10.1007/978-3-540-71041-7
33. Shen, J., Yang, X.F.: Numerical approximations of Allen-Cahn and Cahn-Hilliard equations. Discrete Contin. Dyn. Syst. **28**, 1669–1691 (2010). https://doi.org/10.3934/dcds.2010.28.1669
34. Smith, J.: The coupled equation approach to the numerical solution of the biharmonic equation by finite differences. I. SIAM J. Numer. Anal. **5**, 323–339 (1968). https://doi.org/10.1137/0705028
35. Tang, T., Qiao, Z.H.: Efficient numerical methods for phase-field equations (in Chinese). Sci Sin Math **50**, 775–794 (2020). https://doi.org/10.1360/SSM-2020-0042
36. Toselli, A., Widlund, O.: *Domain decomposition methods—algorithms and theory*, vol. 34 of Springer Series in Computational Mathematics, Springer-Verlag, Berlin, (2005) https://doi.org/10.1007/b137868
37. Wan, Z.S., Guo, B.Y., Wang, Z.Q.: Jacobi pseudospectral method for fourth order problems. J. Comput. Math. **24**, 481–500 (2006)
38. Wang, Z.Q., Wen, X., Yao, G.Q.: An efficient spectral-Galerkin method for elliptic equations in 2D complex geometries. J. Sci. Comput. **95**(89), 26 (2023). https://doi.org/10.1007/s10915-023-02207-4
39. Yang, Z.G., Lin, L.L., Dong, S.C.: A family of second-order energy-stable schemes for Cahn-Hilliard type equations. J. Comput. Phys. **383**, 24–54 (2019). https://doi.org/10.1016/j.jcp.2019.01.014
40. Yao, G.Q., Wang, Z.C., Wang, Z.Q.: A conforming multi-domain Legendre spectral method for solving diffusive-viscous wave equations in the exterior domain with separated star-shaped obstacles. IMA J. Numer. Anal. **45**(6), 3235–3263 (2025). https://doi.org/10.1093/imanum/drae085
41. Yao, G.Q., Wen, X., Wang, Z.Q.: An efficient Fourier-Laguerre spectral-Galerkin method for exterior problems of two-dimensional complex obstacles. Appl. Numer. Math. **193**, 93–108 (2023). https://doi.org/10.1016/j.apnum.2023.07.015
42. Yao, G.Q., Wen, X., Wang, Z.Q.: Efficient spectral methods for PDEs in three-dimensional curved geometries. J. Sci. Comput. **103**(95), 28 (2025). https://doi.org/10.1007/s10915-025-02919-9
43. Yu, X.H., Guo, B.Y.: Spectral element method for mixed inhomogeneous boundary value problems of fourth order. J. Sci. Comput. **61**, 673–701 (2014). https://doi.org/10.1007/s10915-014-9844-y
44. Yue, P.T., Zhou, C.F., Feng, J.J.: Sharp-interface limit of the Cahn-Hilliard model for moving contact lines. J. Fluid Mechanics **645**, 279–294 (2010). https://doi.org/10.1017/S0022112009992679